Identification and Validation of N6-methyladenosine-related Biomarkers for Bladder Cancer: Implications for Immunotherapy

Hongyu Deng
Hunan Cancer Hospital
Faqing Tang
Hunan Cancer Hospital
Ming Zhou
Hunan Cancer Hospital
Dongyong Shan
Central South University Third Xiangya Hospital
Xingyu Chen
Central South University Third Xiangya Hospital
Ke Cao (csucaoke@csu.edu.cn)
Central South University Third Xiangya Hospital https://orcid.org/0000-0001-5392-2306

Research Article

Keywords: Bladder cancer, N6-methyladenosine, tumor immune microenvironment, anti-PD-L1, immune checkpoint inhibitors

Posted Date: December 6th, 2021

DOI: https://doi.org/10.21203/rs.3.rs-1101509/v1

Version of Record: A version of this preprint was published at Frontiers in Oncology on March 2nd, 2022.
See the published version at https://doi.org/10.3389/fonc.2022.820242.

Abstract

N6-methyladenosine (m6A) has emerged as one of the most important modifications of RNA. Based on the expression of 23 kinds of m^6A regulatory factors, we identified three different m^6A modification patterns in bladder cancer. The effects of the three kinds of m^6A modification modes on clinicopathological characteristics, immune cell infiltration level, and gene expression level of immune checkpoint genes were comprehensively analyzed. In addition, the effects of different m^6A modification modes on the therapeutic efficacy of anti-PD-L1 (atezolizumab) are also discussed. Our results confirm that m^6A methylation plays an important role in the immune cell recruitment process in the tumor microenvironment of bladder cancer, which is influences the efficacy of anti-PD-L1 therapy for bladder cancer. We further confirmed the important role of FTO on the biological function of bladder cancer cells by in vitro experiments, FTO functions as an oncogene in bladder cancer cells, and after FTO knockdown, the level of m^6A enzyme activity in bladder cancer cells was significantly increased, apoptosis was increased, and cell proliferation and cell invasion were reduced. In addition, our study also confirmed that K216H and K216E probably are important targets for regulating FTO in the future. We provide new insights into the regulatory pathways of the immune microenvironment and the methylation function of m^6A in bladder cancer, which will help to design novel diagnostic methods, prognostic tools, and therapeutic targets.

1. Introduction

Bladder cancer is the most common cancer of the urinary system and is characterized by a difficult early diagnosis, rapid metastasis, and resistance to treatment. Immune checkpoint therapy (ICT) targets immune pathway effectors such as cytotoxic lymphocyte antigen-4 (CTLA-4), programmed cell death protein 1 (PD-1), or programmed death-ligand 1 (PD-L1)[1]. Anti PD-L1 immunotherapy has been approved by the Food and Drug Administration (FDA) for the treatment of metastatic bladder cancer[2, 3].Immunotherapeutics that target PD-1 or PD-L1 have significantly improved the survival outcomes for some patients, showing an astonishing effect in a small number of patients with sustained efficacy. The improved clinical efficacy for the detection of cancer of the urinary system including advanced-stage bladder cancer has changed the intervention measures used **[4]**; however, some patients with bladder cancer undergoing immunotherapy show no response to ICT or display resistance to drugs, and this scenario does not meet the clinical needs of these patients[5, 6]. At present, multiple studies have confirmed that the immune response resulting due to many tumors, including those found in bladder cancer, is related to the level of immune cell infiltration in the tumor microenvironment, the expression of PD-1/PD-L1, and the tumor mutation burden (TMB)**[7, 8]**.

The microenvironment in which tumor cells grow and survive is called the tumor microenvironment (TME), which includes stromal cells such as cancer-related fibroblasts and macrophages, immune infiltrating cells (myeloid cells and lymphocytes), bone marrow-derived cells (BMDCs) such as endothelial progenitor cells and hematopoietic progenitor cells, and secretory factors such as cytokines **[9]**. There is

mounting evidence that TME plays a crucial role in tumor progression, immune escape, and has an impact on the response to immunotherapy **[10, 11]**. A comprehensive analysis of the heterogeneity and complexity of the TME is a key step in improving the success rate of existing ICTs and the development of new immunotherapy strategies. Further exploration of the regulatory mechanisms underlying TME cell infiltration will improve the ability to guide and predict the response to immunotherapy, and may help identify new therapeutic targets.

N6-methyladenosine (m^6A) is the most common and abundant RNA modification in eukaryotes. As a reversible epigenetic modification, m^6A is found in almost all types of RNAs, including mRNAs, ribosomal RNAs (rRNAs), long noncoding RNAs (lncRNAs), microRNAs (miRNAs), small nuclear RNAs (snRNAs), and circular RNAs (circRNAs), and are dynamically regulated in many physiological processes [12, 13]. The m^6A modification is a dynamic and reversible process in mammalian cells and is regulated by various methyltransferases, demethylases, and binding proteins, also known as writers, erasers, and readers, respectively. The process of m^6A methylation is catalyzed by methyltransferases such as RBM15, ZC3H13, METL3, METL14, WTAP, and KIAA1429, and the removal process is mediated by demethylases such as FTO and ALKBH5 **[14].** Further, a group of specific RNA binding proteins, such as YTHDF1/2/3, YTHDC1/2, HNRNPA2B1, and IGF2BP1/2/3 can recognize the m^6A motif, thus affecting the function of m^6A **[15]**. Results from various studies have shown that the abnormal expression and changes to gene expression for m^6A regulatory factors are related to the dysregulation of multiple biological processes essential for the initiation, progression, metastasis, drug resistance, recurrence, and the immune regulation of cancer **[16]**.

Many studies have confirmed the special correlation between m^6A modification and changes in the TME. Li et al.[17] observed that when METTL3 was depleted, the steady-state growth of T cells was blocked and was maintained at a slow rate. Further, their research showed that METTL3 deletion resulted in a decrease in the level of m^6A, and an increase in the mRNA stability and protein levels of SOCS1, SOCS3, and CISH, thus negatively regulating the IL-7 signal production in $CD4^+$T cells. Results from another study[18] revealed the role of m^6A in dendritic cell activation, in which METTL3 mediated the m^6A modification of the transcripts for the adaptor Tirap for CD40, CD80, and TLR4. Signal adaptors enhanced the translation of METTL3 in dendritic cells, thereby enhancing TLR4/NF-κB signal transduction, producing cytokines, and stimulating T cell activation. From the perspective of immune checkpoint therapy, the m^6A binding protein YTHDF1 can be used to modulate antitumor immunity and improve immunotherapy, as it can regulate the expression of lysosomal proteinase in an m^6A dependent manner. YTHDF1 can recognize the transcription of m^6A modified transcripts, and encodes a lysosomal protease to increase translation in dendritic cells. Moreover, the deletion of *YTHDF1* enhances the cross-presentation of tumor antigens and the cross initiation of $CD8^+$T cells *in vivo*. Further, Wang et al. confirmed that the deletion of *YTHDF1* enhances the therapeutic effect of the PD-L1 checkpoint blockade**[19]**.In melanoma, elevated *FTO* expression levels promote tumor growth by reducing the methylation of m^6A in the mRNA for PD-1 (*PDCD1*), *CXCR4*, and *SOX10* and preventing their RNA decay

mediated by YTHDF2. Knockout of *FTO* in melanoma cells induces tumor cells to become sensitive to interferon-gamma (IFNγ) *in vitro*, and promotes a sensitizing response of melanoma cells to anti-PD-1 antibody in mice[20]. Together, these data prove that the m^{6}A modification plays an important role in regulating the tumor immune microenvironment and the combined use of m^{6}A modulators and PD-1/PD-L1 drugs may prove to be a new strategy to enhance the clinical efficacy of tumor immunotherapy.

In this study, we examined the effect of the m^{6}A methylation modification on the invasion characteristics of immune microenvironment cells and the effect of anti-PD-L1 therapy on bladder cancer. Our study helps elucidate the molecular mechanism underlying the regulation of the immune microenvironment in bladder cancer, and provides new predictors, potential auxiliary targets, and directions for more effective immunotherapy strategies for combating bladder cancer.

2. Material And Methods

2.1 Datasets

The gene expression profile was measured experimentally using the Illumina HiSeq 2000 RNA Sequencing platform at the University of North Carolina The Cancer Genome Atlas (TCGA) genome characterization center. Level 3 data were downloaded from the TCGA data coordination center. This dataset shows the gene-level transcription estimates, i.e., the $\log_2(x+1)$ transformed RSEM normalized counts, and somatic mutation data was downloaded from the site https://portal.gdc.cancer.gov/. IMvigor 210 cohort is a multicenter, single-arm phase II clinical study for evaluating the safety and efficacy of Tecentriq, a PD-L1 inhibitor, in patients with advanced urothelial carcinoma **[21, 22]**. The complete processed expression data detailed clinical annotations, and somatic mutation data was obtained from IMvigor210CoreBiologies, which is a complete documentation software and data package for the R statistical computing environment. The software package is available free of charge under the Creative Commons 3.0 License.

2.2 Consensus clustering for 23 m^{6}A regulators

We identified 23 m^{6}A regulators from published literature**[23, 24]**, including 2 erasers (*ALKBH5*, *FTO*), 13 readers (*FMR1*, *HNRNPA2B1*, *HNRNPC*, *IGF2BP1*, *IGF2BP2*, *IGF2BP3*, *YTHDC1*, *YTHDC2*, *YTHDF1*, *YTHDF2*, *YTHDF3*, *ELAVL1*, *LRPPRC*), and 8 writers (*KIAA1429*, *METTL14*, *METTL3*, *RBM15*, *RBM15B*, *WTAP*, *ZC3H13*, *CBLL1*). The consensus clustering algorithm determined the optimal number of clusters (K value) as 3. Based on the expression of the 23 m^{6}A modulators, different m^{6}A modification patterns were identified by using k-means(based on Euclidean distance), and the patients were classified into three groups for further analysis. We used the consusclusterplus R package to perform the above steps, and performed 1000 iterations (50 iterations, resampling rate of 80%) to ensure the stability of the classification [25].

2.3 Common molecular typing of bladder cancer

We used several published subtype classification systems for bladder cancer, including the Baylor subtype described by Mo et al. **[26]**, who defined urothelial differentiation based on 18 gene markers, thus dividing the muscle-invasive bladder cancers (MIBC) and non-MIBCs (NMIBC) into basal and differentiated subgroups. The UNC of Damrauer et.al. **[27]** identified basal and luminal cancer subtypes by consensus cluster analysis, and further identified 47 genes as predictors of these subtypes. The MDA subtype **[28]** was analyzed by using 2252 genes (2697 probes) from 73 freshly frozen primary MIBC samples, including p53 like, luminal, and basal cancer. The Lund group**[29]** presented a six-class system based on global mRNA expression, including the urothelial-like, genomically unstable, epithelial infiltrated, SCC-like/Mes-like, SCC-like/UroB, and Sc/NE-like cancer. TCGA genotyping**[30]** used 2707 genes to conduct unsupervised cluster analysis on 129 patients with MIBC. The patients were classified into four subtypes (I, II, III, and IV)， using the Cartes d'Identitédes Tumeurs（CIT）-Curie subtypes **[31]**. These classifiers were combined into an R package (BLCAsubtyping) **[32]**, which can be found at https//github.com/cit-BioInfo/BLCAsubtype. We applied these classifiers independently to the TCGA-BLCA cohort and the IMvigor210 cohort to analyze the relationship between the subtypes of different classification methods and three different m^6A modification patterns. Further, we interpreted the differences among the three different m^6A modified subtypes.

2.4 Estimation of TME cell infiltration

We used the single-sample gene set enrichment analysis (ssGSEA) algorithm to quantify the relative abundance of cell infiltration in TME. We obtained gene sets from the data of Qingzhu Jia et al**[33]** to label the different types of TME infiltrating immune cell types. As demonstrated by Jia et al**[33],** we calculated the antitumor-immunity-score as the sum of the immune cell scores of various antitumor cells. Further, the pro-tumor-immunity-score is the sum of the scores of tumor-promoting immune cells, and we define the tumor immunity score as the difference between the pro-tumor-immunity score and the antitumor-immunity-score for unified analysis. In addition, we also used the ESTIMATE algorithm**[34]** to estimate the ratio of the immune matrix components of each sample in the TME to further explore the differences of TME components including immune cells and stromal cells scores among different m^6A modification modes. The results were presented in three forms: immune score, stromal score, and the ESTIMATE score; the higher the score from immune score or stromal score, the more immune or matrix components in TME. The ESTIMATE score is the sum of the immunescore and stromal score, which represents the level of the two components in TME.

2.5 Identification of differentially expressed genes (DEGs) among three types of m6A modified modes

DEGs were identified via the Bayesian method between different m^6A modification modes using the limma R package**[35]**,the absolute value of logFC>1 as the significant criteria. We used the ssGSEA method to score the samples based on the 23 m^6A regulatory factors. Based on the median value of the m^6A score, the patients were classified into a high m^6A score group or a low m^6A score group. The difference between the two groups was analyzed by the empirical Bayes method using the limma R package, taking the corrected p-value<0.05, and the absolute value of logFC>1 as the significant criteria, and 647 DEGs were obtained for subsequent signal pathway analysis.

2.6 Differential signaling pathway enrichment among the three m6A modified modes

The enrichment of signaling pathways for the DEGs expressed relative to the different phenotypes of m^6A were analyzed using the metascape website**[36]** http://metascape.org. We determined the statistically rich terms, accumulated hypergeometric p values, and enrichment factors, and used these in a filtering step. Next, according to the Kappa statistical similarity between the gene members, the remaining important terms were clustered in a hierarchical structure, and the kappa score of 0.3 was used as a threshold to convert the terms to clusters**[36]**. We selected the genes with the best p-value in each cluster as its representative term, and displayed them in the heatmap. The databases for the KEGG pathway, GO biological processes, Reactor gene sets, Canonical pathways, and the CORE resources were used for pathway and process enrichment analysis applying a p-value <0.01, a minimum count of 3, and an enrichment factor>1.5 (the enrichment factor is the ratio between the observed count and the chance expected count). The GSEA analysis**[37]** evaluates the skewness of the two distributions for the selected gene set in the gene list sorted by a specific phenotype. The analysis gene set was obtained from the hallmark gene sets provided by the Molecular Signatures Database (https://www.gsea-msigdb.org/). In this study, we used the clusterProfiler R package to implement the GSEA analysis**[38].**

2.7 Construction of a scoring system to evaluate the level of m^6A modification in individual samples

To quantify the m^6A modification pattern in a single patient, we constructed a scoring system called m^6Ascore based on the mRNA expression level of the 23 identified m^6A regulatory molecules in each sample, and used the ssGESA method to evaluate the m^6A modification pattern in individual bladder cancer patients.

2.8 Analysis of somatic cell copy number of different subtypes

For copy number analysis, we use GISTIC.2 to identify significantly amplified or missing genomes, the burden of copy number loss or gain was calculated as the total number of genes with copy number

changes at the focal and arm levels.

2.9 Relationship between methylation of m^6A and the core biological pathways impacted due to bladder cancer

We analyze a set of gene sets for storing genes related to certain biological processes, and further, to reveal the association between the m^6A gene signature and some related biological pathways, including: (1) the immune-checkpoint; (2) antigen processing machinery; (3) CD8 T-effector signature; (4) epithelial-mesenchymal transition (EMT) markers including EMT1, EMT2, and EMT3; (5) the angiogenesis signature; (7) pan-fibroblast TGF-β response signature (Pan-F-TBRS); (8) WNT targets; (9) DNA damage repair; (10) mismatch repair; (11) Nucleotide excision repair; (12) DNA replication; (13) and antigen processing and presentation.

The differential gene expression of the core biological pathway genes between the different m^6A phenotypes of the IMvigor210 cohort was displayed in the form of a heatmap, including:□A□FGFR3 gene signature;□B□CD8 Teff signature;□C□antigen-processing machinery;□D□immune checkpoint signature; □E□ MKI67 and cell cycle genes;□F□DNA replication-dependent histones;□G□DNA damage-repair genes;□H□ TGFβ receptor and ligand;□I□ F-TBRS genes;□J□EMT markers;□K□angiogenesis signature.

2.10 Cell lines and cell culture

The human bladder cancer cell lines were obtained from the Oncology Institute of Central South University. The cell lines were incubated at 37°C under a humidified atmosphere with 5% CO2 and cultured in DMEM (Invitrogen, CA), added with 10% fetal bovine serum (FBS) (GIBCO, NY), 1 mmol/L glutamine, and 1% penicillin/streptomycin.

2.11 Cell viability, apoptosis, and invasion assay

Cell proliferation was analyzed using a commercial CCK-8 assay kit (#C0038, Beyotime). We employed fluorescence-activated Cell Sorting (FACS) to assess apoptosis with the Annexin V-FITC/PI staining kit (Mbchem). According to the manufacturer, the transwell assay assessed cell invasion with the 6-well insert device (8 μm pore size; Corning Life Sciences, Bedford, MA) and Biocoat Matrigel (BD Biosciences) 's instructions. We calculate the middle and surrounding 5 fields of view and take the average.

2.12 Western blotting

Western blotting was performed as described previously [39]. Briefly, total protein was extracted with RIPA lysis buffer and determined using the bicinchoninic acid (BCA) Protein Assay Reagent Kit. The proteins were separated using 10% SDS-PAGE and electrophoretically transferred into a polyvinylidene fluoride

(PVDF) membrane. The membranes were blocked with 5% skimmed milk powder and incubated overnight at 4°C with primary antibodies targeting FTO(27226-1-AP) and β-actin(1:2000, Ptgcn, 66009-1-Ig) and anti-GAPDH (Abcam, ab125247), followed by incubation with the appropriate secondary antibodies for one h. Positive bands were visualized using an enhanced chemiluminescence system

2.13 Measurement of total m6A assay

Total m^6A content was measured in 200-ng aliquots of total RNA extracted from cells using an m^6A RNA methylation quantification kit (cat. no. P-9005; Epigentek) according to the manufacturer's instructions

2.14 Statistical analysis

The non-paired *t*-test was used to compare the normally distributed variables between the two groups; the Mann-Whitney U test (also known as the Wilcoxon rank-sum test) was used to estimate the statistical significance of the non-normal distribution variables. The Kruskal-Wallis test and a one-way ANOVA were used as nonparametric and parametric analysis methods**[40]**. The correlation coefficient between TME infiltrating immune cells and the expression of m^6A regulatory genes was calculated using the Pearson correlation method. We used the univariate Cox regression model to calculate the risk ratio (HR) for the m^6A regulatory genes. The survminer R software package was used to determine the cut-off point for the correlation between the m^6A scores and patient survival in each data set subgroup. The "surv-cut point" function of the maximum rank statistic was used to double score the m^6A score by repeatedly testing all possible cut-off points, and further, the patients were classified into “high” and “low” subgroups, according to the maximum selected log-rank statistic, to reduce the batch effect in the calculations. The Kaplan-Meier method was used to plot the survival curve for prognosis analysis, and a log-rank test was used to determine the significance of the difference. The waterfall diagram of the maftools software package was used to show the mutations in the 23 m^6A regulatory factors in the TCGA-BLCA cohort. The thermograms of the 23 mutations for the m^6A regulatory factors were plotted. All statistical P-values were bilateral, and $P<0.05$ was considered to be statistically significant.

3. Results

3.1 Survey of 23 m^6A regulatory factors in bladder cancer

In this study, we analyzed 23 m^6A regulatory factors related to bladder cancer, including 2 erasers (*ALKBH5*, *FTO*)、13 readers（*FMR1*, *HNRNPA2B1*, *HNRNPC*, *IGF2BP1*, *IGF2BP2*, *IGF2BP3*, *YTHDC1*, *YTHDC2*, *YTHDF1*, *YTHDF2*, *YTHDF3*, *ELAVL1*, *LRPPRC*）and 8 writers（*KIAA1429*, *METTL14*, *METTL3*, *RBM15*, *RBM15B*, *WTAP*, *ZC3H13*, *CBLL1*）. We first mapped the network for the 23 m^6A regulatory factors in bladder cancer (Fig.1A), and examined the interactions and their significance for the prognosis of bladder cancer patients. We found that there were significant correlations between the expression of m^6A

regulatory factors in writers, erasers, and readers and most of the correlations were positive (Supplementary table1). Based on these correlations, the 23 m^6A regulatory factors were divided into four categories (Clusters A-D). Fig. 1B summarizes the somatic mutation frequency of the 23 m^6A regulators. In 116 out of 412 patient samples, mutation in m^6A regulators were observed, with a frequency of 28.16 %. Most of the mutations were missense mutations, and the regulators *KIAA1429*, *METTL3*, and *ZC3H13* had the highest mutation frequency (4%), while *HNRNPC*, *YTHDF3,* and *FMR1* did not harbor any mutations. Subsequently, we found that *FMR1* and *YTHDF2*, *YTHDF1* and *KIAA1429*, *YTHDF2* and *KIAA1429*, *WTAP,* and *METTL3*, *ZC3H13* and *LRPPRC*, and *ZC3H13* and *YTHDC2* had significant symbiotic relationships (Fig. 1C, P< 0.05). The differential expression analysis for the 23 m^6A regulatory factors in bladder cancer and its adjacent tissues is shown in Fig. 1D. The expression of *ALKBH5*, *FTO*, *METL14*, *WTAP*, *YTHDC1*, *YTHDF3*, and *ZC3H13* in adjacent cancer tissues was significantly higher than that in cancer tissues, while the expression of *METL3*, *YTHDF1*, *YTHDF2*, *ELAVL1*, *IGF2BP1*, *IGF2BP3*, and *HNRNPA2B1* in cancer tissues were significantly higher than those in non-cancerous tissues. However, due to the small sample size of the paracancerous tissues, this result needs further verification. A univariate Cox regression analysis was performed to study the effect of the 23 m^6A regulatory factors on the overall survival (OS) of bladder cancer patients (Fig. 1E). It was observed that six m^6A regulatory factors had a significant effect on the prognosis for bladder cancer patients. *YTHDC1* and *WTAP* may be protective factors (HR<1, P<0.05), while *IGF2BP2*, *ALKBH5*, *IGF2BP3,* and *FTO* are risk factors for bladder cancer (HR>1, P<0.05).

3.2 Three different m^6A methylation modification patterns defined by the 23 m^6A regulatory factors

Based on the gene expression of the 23 m^6A regulatory factors, 407 patients with bladder cancer were classified using the R-package ConsensusClusterPlus. Our analysis showed that 3 clusters were optimal (Fig. 2A-C, Supplementary Fig.1 A-D), and we identified three different m^6A modification patterns in 407 patients with bladder cancer, which we named clusters 1-3. We plotted a heatmap (Fig. 2D) and boxplot (Fig.3A) for the expression of the 23 m^6A regulatory factors in clusters 1-3 and found that the expression of *IGF2BP1*, *IGF2BP1*, *IGF2BP3*, *KIAA1429*, and *RBM15* in cluster2 was lower than in the other clusters (P<0.01), while the expression of *METTL3*, *RBM15B*, *YTHDC1*, *YTHDC2*, *YTHDF1*, *YTHDF2*, *YTHDF3*, and *ELAVL1* was higher in cluster2 than the other clusters. Significant overall survival were found in the patients who had m^6A modifications from cluster2 (Fig.3B). To better understand the potential differences between the three m^6A modification patterns, we compared them with the published molecular typing of bladder cancers, including Baylor, MDA, CIT-Curie, and UNC (Fig.3C). Using the CIT classification, Cluster1 and 3 showed more MC7 subtypes, and more MC1 subtypes were seen in cluster2; Using the Baylor classification, cluster1 and cluster3 had more basal subtypes, and cluster2 contained more differentiated subtypes; based on the UNC classification, the basal subtype was more frequent in cluster1 and cluster3 than the luminal subtype, while cluster2 showed the opposite result. To further

characterize the molecular differences between the RNA based subtypes, we analyzed the expression of 23 regulatory genes associated with bladder cancer **[41-47]**, including the steroid hormone receptors ESR1/2, AR and PGR, the nuclear receptors PPARG, three RARs (A/B/G), and three RXRs (A/B/G), the receptor tyrosine kinases ERBB2/3 and FGFR1/3, and the transcription factors FOXA1, FOXM1, GATA3/6, HIF1A, KLF4, STAT3, and TP63We found significant differences in the expression of most regulators between cluster2 and the other two m^6A subtypes. The expression of *RARG*, *FGFR3*, *RXR3*, *FOXA1*, *ERBB3*, *AR*, *ERBB2*, *PPARG*, *GATA3*, *ESER2*, and *RXRB* in cluster2 was significantly higher than that in cluster1 and cluster3, while the opposite relation was found for *STAT3*, *FOXM1*, *EGFR*, *HIF1A*, *GATA6*, *FGFR1*, and *RARB* (Fig.3D). Further, we identified differences in the mutation of 20 genes in the three m6A modification modes as shown in the waterfall diagram (Supplementary Fig.1E). and we analyzed the difference in Copy number alterations across three m6A modification modes. (Supplementary Fig.2,3).

3.3 Difference in immune cell infiltration characteristics in the tumor immune microenvironment for different m^6A modification modes

To reveal the role of m^6A modification-related phenotypes in TME immunoregulation, we calculated the abundance of 28 cellular subsets in each patient sample. The heatmap shows the average difference in the infiltration level of 28 types of immune cells in the three different m^6A modification modes (Fig. 4A, Supplementary table2-3),We found significant differences in the characteristics of cellular infiltration in the TME; cluster2 is characterized by immunosuppression, and most of the infiltrating cells are immune cells .The infiltration level was significantly lower than that of cluster1 and cluster3 (Supplementary Fig.4A). In addition, the anti-tumor immunity score and the pro-tumor immunity score of cluster2 was significantly lower than that of cluster1 and cluster3 (Supplementary Fig.4B and C), and the pro-tumor score of cluster2 is significantly higher than in cluster1 and cluster3 (Fig. 4B). The ESTIMATE algorithm can estimate the ratio of the immune and matrix components of each sample in the TME, which is presented in the form of three scores: the immune score, stromal score, and the ESTIMATE score. We found that the 3 scores in cluster2 were significantly lower than those in cluster1 and cluster3 (Fig.4C), suggesting that m^6A methylation may be involved in regulating the type of TME infiltrating cells and play a central role in immune regulation. However, the mechanism for how m^6A modification affects the immunophenotype is unclear. Therefore, we analyzed the correlation between the 23 m^6A regulatory factors and the 28 types of immune cells (Fig.4D). A heatmap of the correlation showed that the m^6A regulators were highly correlated with most of the immune cells, and *WTAP*, *IGF2BP2*, and *IGF2BP3* showed the most significant correlation with most immune cells. Further, *YTHDF2*, *YTHDC1*, *METTL3*, and*ELAVL1* showed a high negative correlation with most immune cells, indicating that these regulators may play an important role in the differentiation and recruitment of immune cells. To further explore the possible role of m^6A related phenotypes in immunotherapy, we studied the difference in the expression of the immune checkpoint related genes *CD274*, *PDCD1LG2*, *CTLA4*, *LAG3*, *PDCD1*, *HAVCR2*, *TIGIT*, and the CD8+T cell marker genes including *CD8A*, *GZMB*, *CXCL9*, *CXCL10*, *PRF1*, *TBX21*, and *CD8B* in the three different m6A modification modes (Fig. 4e, F). Our results showed that the expression of these genes in

cluster2 was significantly lower than that in cluster1 and cluster3 (P< 0.0001). The results suggest that m^6A methylation affects the type of TME infiltrating cells, and cluster2 had a significantly lower level of immune cell infiltration related to the immune checkpoint than the other two modification modes. The gene expression in cluster2 is significantly low, and we speculated that the response to immunotherapy in patients showing cluster2 type m^6A modifications may be worse than that of cluster1 and cluster3.

3.4 Enrichment of DEGs and the signaling pathways involved in the different m^6A modification modes

To reveal the potential biological differences among the three different m^6A modification patterns, we undertook an expression profiling of the patient tissue samples and identified 403 DEGs (Fig.5A). The Circos diagram shows the overlap of the DEGs obtained by a pairwise comparison of the three different m^6A modification modes. Cluster2 had more DEGs than cluster 1, and there are more gene overlaps in the list of DEGs obtained for cluster1 compared with cluster2, and between cluster3 and cluster2 (Fig. 5B). In Fig. 5B, the blue lines connect genes belonging to the same ontology term showing the number of functional overlaps between different groups.

We used Metascape[36] to analyze the enrichment of signaling pathways between the different m^6A modification classes. The results are shown in the heatmap which is colored by p-values, and the white cells indicate a lack of enrichment of the term in the corresponding gene list (Fig. 5C, D, and Supplementary Fig. 5A, B). Additionally, a GSEA was performed for further signal pathway enrichment analysis (Figure 5E),IL2/STAT5 signaling, EMT, inflammatory response, interferon-gamma response, and TNFα signaling via NFκB are enriched in cluster1. Allograft, Rejection, Complement, EMT, Ransition, Inflammatory Response,Kras Signaling Dn are enriched in cluster3. These signaling pathways involve different core biological processes, most of which are related to the regulation of immunity, and some of them have been confirmed to have a correlation in immunotherapy **[48-50]**, which provides a basis for further exploration of the effect of m^6A modifications on the immunophenotype.

3.5 The m^6A score is an important prognostic biomarker and predictor of bladder cancer

We constructed and evaluated a scoring system called the m^6Ascore to quantify the level of m^6A modification in each patient sample, taking into account the individual differences and complexity of the m^6A modification. First, we conducted a survival analysis using the m^6Ascore and found that patients with high m^6Ascore had a poor prognosis (p=0.036, Fig. 6A). There were also significant differences in the m^6Ascore among the three different m^6A modification modes, with the lowest and highest m^6Ascores being assigned to cluster3 and cluster2, respectively (Fig. 6B). Next, we analyzed the differences in m^6Ascore in the MDA cancer subtype and found the highest score for the basal subtype, followed by the

luminal subtype, with the lowest expression level observed in the p53-like subtype (Fig. 6C). To explore the potential biological relevance of m^{6}Ascore, we classified 407 patients into a high m^{6}Ascore group and a low m^{6}Ascore group based on the expression level of the 23 m^{6}A regulators. We first examined the difference in the composition of immune cells between the two patient groups (Fig. 6D). Our results showed that CD56^{dim} natural killer cells, central memory CD4T cells, eosinophils, mast cells, monocytes, and type 17 T helper cells showed a significantly low enrichment in the high m^{6}Ascore group. Further, the activated CD4$^+$ T cells, memory B cells, natural killer T cells, neutrophils, and type 2 T helper cells showed a highly significant enrichment in the low m^{6}Ascore group. We analyzed the DEGs, and additionally examined the signaling pathways showing enrichment via GO and KEGG pathway analysis between the two groups. The pathways showing enrichment for molecular function (MF), cellular component (CC), and biological process (BP) via GO analysis were examined. Signaling pathways enriched for BP include the xenobiotic metabolic process, hormone metabolic process, epidermis development, etc.; pathways enriched for CC included the apical part of the cell, apical plasma membrane, cornified envelope, etc.; and pathways enriched for MF include monooxygenase activity, serine-type endopeptidase activity, and other signaling pathways (Supplementary Fig. 5C-E). A KEGG pathway analysis showed that the DEGs were mainly enriched in glutathione metabolism, ether lipid metabolism, and other signaling pathways (Supplementary Fig. 5F). A GSEA analysis (Fig. 6E-F) showed that pathways for the inflammatory response, interferon-gamma response, myc targets V1, TNFα signaling via NFκB, and other genes were concentrated in high m^{6}Ascore group. These results strongly suggest a significant correlation between a high m^{6}Ascore and immune activation. The results also demonstrate the central role of m^{6}A methylation in different biological processes in bladder cancer, including different aspects of immune regulation. The m^{6}Ascore may be used to evaluate the characteristics of immune cell infiltration in bladder cancer tissue to predict the clinical response of patients to immunotherapy. Thus, the m^{6}Ascore may have the potential to be used as an independent prognostic biomarker to predict the OS rate of patients, guiding more effective clinical practice.

3.6 Effect of m^{6}A methylation modification on anti-PD-L1 immunotherapy for bladder cancer

To explore the potential effect and mechanism of m^{6}A methylation on immunotherapy for bladder cancer, we obtained data for the IMvigor210 cohort, which is an open-label, multicenter, single-arm phase II clinical study to evaluate the safety and efficacy of Tecentriq, an anti-PD-L1 agent, in patients with advanced urothelial cancer(Supplementary table4). Patients who responded in whole or in part were classified as responders, and were compared with non-responders who showed the incidence of stable or progressive disease. We performed an unsupervised clustering using data for mRNA expression for the 23 m^{6}A regulatory factors from all patients. A consensus clustering approach based analysis indicated the optimal number of clusters as 3 (Supplementary Fig.6A-D). We identified three different m^{6}A modification patterns and calculate the m^{6}Ascore for subsequent analysis. Additionally, we performed a

combined heatmap based analysis (Fig. 7) to find the correlation between the different m^{6}A methylation modes and the Lund and TCGA molecular typing for the anti-PD-L1 based immunotherapy. Further, for the three groups of m6A methylation modification patterns, we also analyzed the differences in PD-L1 expression in immune cells (IC) and tumor cells (TC), patients' response to anti-PDL1 efficacy, TMB, m^{6}Ascore, and the important gene mutations prevalent in bladder cancer. We also analyzed the differences in the expression of genes in important biological pathways for bladder cancer[51], including the *FGFR3* gene signature; CD8 Teff signature; antigen-processing machinery; immune checkpoint signature; MKI67 and cell cycle genes; DNA replication-dependent histones; DNA damage-repair genes; TGFβ receptor and ligand; F-TBRS genes; EMT markers; and the angiogenesis signature. In the comparison between the different m^{6}A modification patterns and the TCGA and Lund classification using a heat map based analysis, we found that most genes in cluster1 classified as subtype I and the least as subtype IV. For the Lund classification, we observed that the UroA subtype had the highest proportion in cluster1, the Inf type has the highest proportion in cluster2, and the SCCL subtype was more enriched in cluster1. Additionally, we found that the cluster3 modification mode had higher levels of PD-L1 expression in immune cells and tumor cells, a higher proportion of CR/PR (Fig. 7, Fig. 8A). These results suggest that m^{6}A methylation may be involved in the response to anti-PDL1 therapy. Additionally, among the three different m^{6}A methylation modes in bladder cancer, there were differences in gene mutations[51]for *TP53*, *RB1*, *FGFR3*, *CDKN2A*, *ERBB2*, and *PIK3CA*. Patients had a greater number of *FGFR3* and *CDKN2A* mutations in cluster1 than in cluster1 or cluster2, while the converse was true for *TP53* mutations. There were significant differences among the three m^{6}A methylation patterns in most gene sets. The expression of the *FGFR3* gene signature (*FGFR3*, *TP63*, *WNT7B*) in cluster1 was significantly higher than in the other two groups, while the CD8 Teff signature (*CD8A*, *GZMA*, *GZMB*, *PRF1*, *CXCL9*, *CXCL10*, *TBX21*),antigen-processing machinery (*TAP1*, *TAP2*, *B2M*, *HLA-A*, *HLA-B*, *HLA-C*), and the immune checkpoint signature (*CD274*, *PDCD1LG2*, *CTLA4*, *PDCD1*, *LAG3*, *HAVCR2*, and *TIGIT*) are less expressed in cluster1 than the other two modification modes, and are highly expressed in the cluster3 subgroup. The CD8 Teff and the immune checkpoint signatures are often used to predict the efficacy of immunosuppression in patients with immune checkpoint suppression; a higher expression level is linked to better clinical outcomes**[5, 52]**. Additionally, our results indicated that the expression of *MKI67* and cell cycle genes□DNA replication-dependent histones; DNA-repair genes is significantly higher in cluster3; TGFβ receptor and ligand; F-TBRS genes; EMT markers; angiogenesis signature show significantly increased gene expression in cluster2. We have observed that there are more compact types and fewer read types in cluster1. Compared with Lund typing, there are more SCCL types in cluster1, more UroA types in cluster1, and more infs types in cluster2 (Fig. 8A). We found differences in m^{6}Ascore levels among the three m^{6}A modification modes, with the lowest m^{6}Ascore level found in cluster2, while the m^{6}Ascore of cluster3 and cluster1 were the same, with no significant difference (Fig. 8B). Differences in the m^{6}Ascore were also observed in immunophenotyping, with the excluded subtype having the highest m^{6}Ascore, and no significant difference in m^{6}Ascore found between the inflamed and desert subtypes (Fig. 8C).

Next, we analyzed the correlation between m^6Ascore and biological pathway gene scores[39] in bladder cancer (Fig. 8D). The m^6Ascore was positively correlated with the scores for DNA replication, mismatch repair, Fanconi, base excision repair, nucleotide excision repair, homologous recombination, cell cycle, and DDR, and negatively correlated with EMT2, EMT1, immune checkpoint, CD8 T effector, APM, etc. The effect of the m^6Ascore on OS was observed by plotting the KM curve, which indicated that a higher m^6Ascore had a poor prognosis (P=0.032Fig. 8E). Using the SubMAP algorithm, we inferred the possibility of anti-PD1 and anti- cytotoxic T-lymphocyte-associated protein 4 (CTLA4) response immunotherapy in the high and low m6Ascore groups. High ICscore group may respond better to PD-1 treatment (Bonferroni-corrected P = 0.03Fig. 8F).

3.7 *FTO* may be play an important role in anti-PD-L1 immune checkpoint therapy.

The results from our data analysis showed that patients with high expression of *FTO* had a poor prognosis in the IMvigor210 cohort (p=0.0035; Fig. 9A), and there were differences in *FTO* expression in the three groups (Fig. 9B). We also queried the predictive value of *FTO* expression in the cohort for anti-PD-L1 immunotherapy, and found that there was a significant difference in *FTO* expression between non-responders and objective remission groups. Non-responsive patients showed significantly higher *FTO* expression (Fig. 9C), suggesting that *FTO* may play an important role in the anti-PD-L1 treatment of bladder cancer. Upon further examination, *FTO* expression was positively correlated with the EMT signaling pathway and negatively correlated with the DDR/cell cycle, nucleotide excision repair, Fanconi anemia pathway, and other signaling pathways (Fig. 9D), and additionally, was negatively correlated with the protein level of PD-L1 in immune cells (Fig. 9e). *FTO* had no significant correlation with the total PD-L1 level in tumor cells (Fig. 9F). The analysis of data from the TCGA database showed that the prognosis of patients with a high expression of *FTO* was worse (p=0.0015; Fig. 9G), and *FTO* expression was higher in patients with a high stage of bladder cancer (Fig. 9H). Additionally, the enrichment results of *FTO*-related gene pathways showed that *FTO* may be involved in the regulation of focal adhesion, the Hippo signaling pathway, the TGF-β signaling pathway, and other signal pathways (Fig. 9I). Previous studies have confirmed that the activation of EMT and TGF-β related pathways reduces T cell migration to tumors and weakens their tumor-killing effect[5, 51]. Therefore, *FTO* may play an important role in the occurrence and development of bladder cancer, the efficacy of anti-PD-L1 immune checkpoint therapy, and may be useful for predicting the prognosis.

To further understand the role of *FTO* in bladder cancer, we explored the mutations that may affect its function. The overall mutation level of *FTO* was 0.97%, and included mainly missense and nonsense mutations (Supplementary Fig. 7A). We found that no correlation existed between *FTO* expression and the level of *PDCD1* (PD-1) and *CD274* (PD-L1) mRNAs (Supplementary Fig. 7B-C), and significant differences in *FTO* expression were found between cancerous and paracancerous tissues in multiple patients (Supplementary Fig7. D). The expression of *FTO* in paracancerous tissue in bladder cancer was higher than in cancer tissues, but due to the relatively small number of paracancerous tissue samples in

the TCGA database, these findings need additional data to support them. An analysis of the correlation between *FTO* and the level of cell infiltration in the tumor immune microenvironment in 32 cancer species indicated a high correlation between *FTO* expression and the immune cells of COAD, THCA, and other cancer species (Supplementary Fig. 7E). Additionally, a high correlation between *FTO* expression and the ESTIMATE score, immune score, and stromal scores of multiple cancer species was observed (Supplementary Fig. 7F). Radar maps showing the correlation between *FTO* expression and the TMB in multiple cancer species (Supplementary Fig. 7G) and microsatellite instability (MSI) are shown (Supplementary Fig. 7H).

3.8 FTO may be involved in the occurrence and development of bladder cancer.

We examined the nuclear, cytoplasmic, and overall expression levels in nine human bladder cancer cell lines: BIU87 cells, 5637 cells, T24 cells, EJ cells, RT4 cells, J82 cells, UM-UC-3 cells, TCCSUP cells, and human bladder epithelial immortalized SV-huv-1 cells (Fig. 10A). IF immunofluorescence detected FTO protein localization in two FTO high expressing cell lines (EJ and T24 cells) and two FTO low expressing cell lines (BIU87 and RT4). We found that FTO was expressed in both cytosol and cytosol of these cell lines (Fig. 10B). Subsequently, we knocked down the FTO of EJ and RT4 by siRNA. CCK-8 examination revealed that cell proliferation was reduced in the si-FTO group (Fig. 10C), and transwell assays observed reduced cell invasion in the si-FTO group (Fig. 10D). Flow cytometry revealed increased apoptosis after knockdown of FTO (Fig. 10E). The level oftotal cellular FTO-M6A enzyme activity was significantly increased (Fig. 10F), and total FTO protein was decreased in the si-FTO group (Fig. 10G). These results confirm the critical role of FTO in bladder cancer.

According to our previous study[53], we confirmed the existence of important modification sites K216 for FTO protein, including K216R, K216H, K216S, and K216E. We constructed plasmids and transfected them into BIU87 and RT4 cells, as well as detected the expression of FTO protein in each group by WB (Fig. 11A). The apoptosis was increased in the FTO-MT(K216H) and MT(K216E) groups (Fig. 11B), and the cell invasion was significantly reduced in the FTO-MT(K216H) and MT(K216E) groups as observed by transwell assay (Fig. 11C), and the total FTO-M6A enzyme activity level was significantly increased in these two groups (Fig. 11D). The above results suggest that K216H and K216E may be important targets for regulating FTO in the future.

4. Discussion

More than 150 RNA modifications have been identified in all organisms, including 5-methylcytosine (m^5C), N6-methyladenosine (m^6A), and N1-methyladenosine (m^1A), of which the m^6A RNA methylation is considered to be the most prominent and abundant form of internal modification in eukaryotic cells**[54]**. The study of m^6A modification in cancer is a new field of cancer research, which may reveal a new layer of epigenetic regulation in cancer, and provide new insights into the tumorigenesis, immune

response, and the molecular mechanisms underlying drug resistance during therapy. Additionally, it may lead to the development of new, effective treatments**[55]** through the use of effective inhibitors targeting maladjusted m^6A regulatory factors alone (or editing targeted mutant or dysfunctional m^6A sites through targeted transcriptomics), or in combination with other therapies. Targeting the m^6A modification may have a strong therapeutic potential for the treatment of all types of cancers, especially those that are resistant to existing treatments**[56].**

Due to technical and resource constraints, most studies have focused on a single TME immune cell type or a single m^6A. The overall infiltration characteristics of the TME mediated by the combined effects of multiple m^6A regulators have not been widely analyzed**[57, 58].** The modification of m^6A is a reversible process that is affected by various writers, erasers, and readers. In this study, we explored the effects of multiple m^6A regulators on the infiltration of immune cells in the TME of bladder cancer, the molecular mechanisms underlying m^6A modification in bladder carcinogenesis, the immune response, and the drug resistance of immune checkpoint inhibitors. We also provide new insights into the role of m^6A modification modes in TME cell infiltration and developing more effective immunotherapy strategies.

We classified patients with bladder cancer based on the expression of 23 m^6A regulatory molecules, and identified three different m6A methylation patterns. We found that cluster2 showed unique specificity compared with the other two types. A quantification of 28 immune cells in the immune microenvironment of bladder cancer using the ssGSEA algorithm showed that cluster2 had a low level of immune cell infiltration characterized by immune inhibition, which corresponds to the immune desert phenotype. Furthermore, an analysis performed using the ESTIMATE algorithm showed that the stromal and immune scores in cluster2 were lower than the other two subtypes, which corroborates our previous results. The expression of immune checkpoint and $CD8^+$T cell markers were lower in cluster2 than in the other two groups, and studies have shown that the expression of these markers is highly sensitive to immune checkpoint inhibitors**[52]**. Thus, different m^6A methylation modification patterns are significantly related to immune activation, and a comprehensive evaluation of the m^6A modification pattern will enable the understanding of the characteristics of TME cell infiltration. An analysis of DEGs between the different m^6A modification modes uncovered m^6A-related signaling pathway genes. These were mainly enriched in the biological pathways related to the matrix and immune activation. In the anti-PD-L1 treatment cohort, we identified three different m^6A methylation patterns, and found significant differences in gene expression and mutations in biological pathway genes associated with the three subtypes of bladder cancer. We constructed a scoring system to quantify and evaluate the m^6A modification level in a single tumor, and found that a high m^6Ascore was related to poor prognosis in the TCGA and anti-PD-L1 cohorts. Patients with a high or low m^6Ascore showed differences in immune cell infiltration in the tumor immune microenvironment. A GSEA signaling pathway analysis indicated that the high and low m^6Ascore are mainly enriched in the matrix and immune-related signaling pathways. Together, these results indicate that the m^6A score is a reliable tool for the comprehensive evaluation of m^6A modification patterns in tumors in individuals, and to determine the mode of infiltration in the TME. The

expression and gene changes for m6A regulatory factors are related to a variety of biological processes, especially the matrix and immune activation. Our findings may provide new impetus for improving the clinical response of patients with bladder cancer to immunotherapy, the identification of different immunophenotypes in bladder cancer, and for promoting individualized immunotherapy.

The role of *FTO* in cancer has recently garnered increasing attention. Previous studies conducted by our group have shown that *FTO*-mediated m^6A modification plays an important role in hepatocellular carcinoma, and the SIRT1 deacetylase can play a carcinogenic role by down-regulating *FTO***[59]**. *FTO* is an RNA demethylase which can remove the methyl of m^6A in mRNA both *in vitro* and *in vivo***[60, 61].***FTO* has catalytic demethylation activity for both cap-m^6Am and internal m^6A. As the abundance of m^6A in mRNA is much higher than that of its preferred binding target m^6Am, the main target of *FTO* is m^6A**[62].** Reports indicate that the *FTO*-mediated demethylation of cap-m^6Am leads to mRNA degradation**[63],** but the evidence for this is inconsistent. PCIF1 is the cap-m^6Am methyltransferase, which processes cap-m^6A alone but not internal m^6A. Reports indicate that the cap-m^6Am added by PCIF1 does not change the level of gene expression or the stability of transcripts**[64-66]**. Additionally, studies**[67]** have found that the spatial distribution of *FTO* can also play a regulatory role. The N-terminus of FTO has an NLS, which can be partially distributed in the nucleus and the cytoplasm, and the distribution of FTO is different in different cell lines, its role and regulation being affected by the environment. Yang et al**[20]** have shown that the induction of *FTO* can be used as an adaptive mechanism to combat metabolic stress in melanoma cells, thus increasing their proliferation, invasion, and migration, and promoting the tumorigenesis and development of melanoma in mice. Further, the authors showed that an *FTO* knockout can increase m^6A methylation in key oncogenic melanoma cells, including the loci for PD-1 (*PDCD1*), *CXCR4*, and *SOX10*. The inhibition of *FTO* makes melanoma cells sensitive to interferon-γ (IFN-γ) and anti-PD-1 therapy in mice, indicating that *FTO* plays an important role in promoting the occurrence of melanoma and anti-PD-1 drug resistance. The role of m^6A involvement with *FTO* in bladder cancer had not been reported, and we found that in the TCGA and IMvigor210 cohorts, patients with high *FTO* expression had a poor prognosis, and the expression of *FTO* was higher in patients with a higher stage of bladder cancer.

In addition, we analyzed the predictive value of *FTO* expression in the cohort subjected to anti-PD-L1 immunotherapy, and found that there was a significant difference in *FTO* expression between the non-responders and the objective remission group. The level of *FTO* expression in the patients non-responsive to anti-PD-L1 therapy was significantly higher than in patients in remission. The data showed that *FTO* expression was negatively correlated with the protein level of PD-L1 in immune cells (Fig. 9e), was positively correlated with the EMT signaling pathway, and negatively correlated with DDR, cell cycle, nucleoside exercise repair, fanconi anemia pathway, and other signaling pathways. The enrichment of *FTO* related gene pathways indicated that *FTO* might be involved in the regulation of focal adhesion/Hippo signaling pathway/TGF-β signaling, these results suggest that *FTO* plays an important role in bladder cancer. The combination of *FTO* targeted regulation and anti-PD-L1 blockers may have great therapeutic potential for reducing the resistance of bladder cancer to immunotherapy. Thus, this

study furthers the understanding of the regulation of m^6A modification in the tumor immune microenvironment of bladder cancer, and contributes to the potential development of new predictive indicators, drug combination strategies, and new immunotherapeutic strategies for cancer immunotherapy. However, its specific role and mechanism need further experimental study.

In this study, we systematically analyzed the mutation and correlation of 23 kinds of m^6A regulatory factors in bladder cancer, and their effects on OS and immune invasion, We found three different patterns of m^6A modification and compared them with other important molecular types of bladder cancer, such as MDA, Lund and Baylor the effects of the three kinds of m^6A modification modes on the mutation characteristics, clinicopathological characteristics, gene expression, immune cell infiltration level, and gene expression level of immune checkpoint regulators were comprehensively analyzed. Further, we investigated the effect of m^6A modification mode on the therapeutic efficacy of bladder cancer immune checkpoint inhibitor anti-PD-L1. Our results confirmed that m^6A methylation is involved in the process of immune cell recruitment in the TME of bladder cancer, and may affect the efficacy of anti-PD-L1 therapy. In addition, we established a method to quantify the level of m^6A modification (m6Ascore), which we found to be an important and powerful prognostic biomarker and predictor for bladder cancer. Thus, this study furthers the understanding of the regulation of m^6A modification in the tumor immune microenvironment of bladder cancer, and contributes to the potential development of new predictive indicators, drug combination strategies, and new immunotherapeutic strategies for cancer immunotherapy.

Conclusion

This study comprehensively recognized the role of m^6A methylation modification on the invasion characteristics of bladder cancer immune microenvironment cells, and the effect on the anti-PD-L1 treatment for bladder cancer. The difference in m^6A modification mode is an important factor indicating the heterogeneity and complexity of the tumor microenvironment, and the immunotherapy impact. The m^6A modification mode helps decipher the molecular mechanisms underlying the immune microenvironment regulation in bladder cancer, and provide new predictive indicators, possible auxiliary targets, and directions for guiding more effective immunotherapy strategies in the future.

Abbreviations

m^6A: N6-methyladenosine;

TCGA: The Cancer Genome Atlas;

GEO: Gene-Expression Omnibus;

KEGG: Kyoto encyclopedia of gene and genome

GO: Gene ontology

GSEA: Gene set enrichment analysis

SsGSEA: The single-sample gene set enrichment analysis

TME: Tumor microenvironment

TMB: Tumor mutation burden

ICT: The immune checkpoint therapy

CTLA-4: Cytotoxic lymphocyte antigen-4

PD-1: Programmed cell death protein 1

PD-L1: Programmed-death ligand 1

DCs: Dendritic cells;

DEGs: Differentially expressed genes;

EMT: Epithelial-mesenchymal transition;

ICB: Immunological checkpoint blockade;

TGFb: Transforming growth factor beta;

Declarations

Authors contributions

XYC and KC designed the study, XYC,DH and MQX analyzed and interpreted the data, XYC,YXZ,LG,HL AND YXC wrote this manuscript. YJ,ZWW,XML and QT edited and revised the manuscript.All aythors have seen and approved the final version of the manuscript.

Acknowledgements

We thank our colleagues in the department of laboratory medicine for helpful discussions and valuable assistance.

Conflicts of interest

The authors have declared that no conflict of interest exists.

Consent for publication

All authors have agreed on the contents of the manuscript.

Funding

This work was supported by Supported by the science and technology innovation Program of Hunan Province(2020RC2066), Hunan Provincial Natural Science Foundation of China(2020JJ5335), Science and Technology Foundation of Changsha City(kq1907127), Health Commission Science Foundation of Hunan Province(20200957), Hunan Cancer Hospital Climb Plan(QH201904),the science and technology innovation Program of Hunan Province (2021RC204),the National Science Foundation of China (81874137).

Authors' contributions

HYD, XYC and KC designed the study, HYD and FQT analyzed and interpreted the data, HYD, FQT and MZ wrote this manuscript. HYD, FQT, MZ and DYS edited and revised the manuscript. All authors have seen and approved the final version of the manuscript.

Ethics approval and consent to participate

The experimental protocol was established, according to the ethical guidelines of the Helsinki Declaration and was approved by the Human Ethics Committee of Ethical Review Committee of the Third Xiangya Hospital of Central South University. Written informed consent was obtained from individual or guardian participants.

Availability of data and materials

All data used in this work can be acquired from the GDC portal (https://portal.gdc.cancer.gov/) and the IMvigor210CoreBiologies http://research-pub.gene.com/IMvigor210CoreBiologies

References

1. Herbst RS, Soria JC, Kowanetz M, Fine GD, Hamid O, Gordon MS, Sosman JA, McDermott DF, Powderly JD, Gettinger SN, et al: **Predictive correlates of response to the anti-PD-L1 antibody MPDL3280A in cancer patients.** *Nature* 2014, **515:**563-567.

2. Inman BA, Longo TA, Ramalingam S, Harrison MR: **Atezolizumab: A PD-L1-Blocking Antibody for Bladder Cancer.** *Clin Cancer Res* 2017, **23:**1886-1890.

3. Powles T, Eder JP, Fine GD, Braiteh FS, Loriot Y, Cruz C, Bellmunt J, Burris HA, Petrylak DP, Teng SL, et al: **MPDL3280A (anti-PD-L1) treatment leads to clinical activity in metastatic bladder cancer.** *Nature* 2014, **515:**558-562.

4. Davis AA, Patel VG: **The role of PD-L1 expression as a predictive biomarker: an analysis of all US Food and Drug Administration (FDA) approvals of immune checkpoint inhibitors.** *Journal for*

Immunotherapy of Cancer 2019, **7**.

5. Gomez de Liano Lista A, van Dijk N, de Velasco Oria de Rueda G, Necchi A, Lavaud P, Morales-Barrera R, Alonso Gordoa T, Maroto P, Ravaud A, Duran I, et al: **Clinical outcome after progressing to frontline and second-line Anti-PD-1/PD-L1 in advanced urothelial cancer.** *Eur Urol* 2020, **77:**269-276.

6. Wolacewicz M, Hrynkiewicz R, Grywalska E, Suchojad T, Leksowski T, Rolinski J, Niedzwiedzka-Rystwej P: **Immunotherapy in Bladder Cancer: Current Methods and Future Perspectives.** *Cancers (Basel)* 2020, **12**.

7. Bellmunt J, Powles T, Vogelzang NJ: **A review on the evolution of PD-1/PD-L1 immunotherapy for bladder cancer: The future is now.** *Cancer Treat Rev* 2017, **54:**58-67.

8. Schneider AK, Chevalier MF, Derre L: **The multifaceted immune regulation of bladder cancer.** *Nat Rev Urol* 2019, **16:**613-630.

9. Tang H, Wang Y, Chlewicki LK, Zhang Y, Guo J, Liang W, Wang J, Wang X, Fu YX: **Facilitating T Cell Infiltration in Tumor Microenvironment Overcomes Resistance to PD-L1 Blockade.** *Cancer Cell* 2016, **29:**285-296.

10. Binnewies M, Roberts EW, Kersten K, Chan V, Fearon DF, Merad M, Coussens LM, Gabrilovich DI, Ostrand-Rosenberg S, Hedrick CC, et al: **Understanding the tumor immune microenvironment (TIME) for effective therapy.** *Nat Med* 2018, **24:**541-550.

11. Tsukamoto H, Fujieda K, Miyashita A, Fukushima S, Ikeda T, Kubo Y, Senju S, Ihn H, Nishimura Y, Oshiumi H: **Combined Blockade of IL6 and PD-1/PD-L1 Signaling Abrogates Mutual Regulation of Their Immunosuppressive Effects in the Tumor Microenvironment.** *Cancer Res* 2018, **78:**5011-5022.

12. Dai D, Wang H, Zhu L, Jin H, Wang X: **N6-methyladenosine links RNA metabolism to cancer progression.** *Cell Death Dis* 2018, **9:**124.

13. Tuncel G, Kalkan R: **Importance of m N(6)-methyladenosine (m(6)A) RNA modification in cancer.** *Med Oncol* 2019, **36:**36.

14. Malla S, Melguizo-Sanchis D, Aguilo F: **Steering pluripotency and differentiation with N(6)-methyladenosine RNA modification.** *Biochim Biophys Acta Gene Regul Mech* 2019, **1862:**394-402.

15. Zhang Z, Luo K, Zou Z, Qiu M, Tian J, Sieh L, Shi H, Zou Y, Wang G, Morrison J, et al: **Genetic analyses support the contribution of mRNA N(6)-methyladenosine (m(6)A) modification to human disease heritability.** *Nat Genet* 2020.

16. Wang S, Sun C, Li J, Zhang E, Ma Z, Xu W, Li H, Qiu M, Xu Y, Xia W, et al: **Roles of RNA methylation by means of N(6)-methyladenosine (m(6)A) in human cancers.** *Cancer Lett* 2017, **408:**112-120.

17. Li HB, Tong J, Zhu S, Batista PJ, Duffy EE, Zhao J, Bailis W, Cao G, Kroehling L, Chen Y, et al: **m(6)A mRNA methylation controls T cell homeostasis by targeting the IL-7/STAT5/SOCS pathways.** *Nature* 2017, **548:**338-342.

18. Wang H, Hu X, Huang M, Liu J, Gu Y, Ma L, Zhou Q, Cao X: **Mettl3-mediated mRNA m(6)A methylation promotes dendritic cell activation.** *Nat Commun* 2019, **10:**1898.

19. Han D, Liu J, Chen C, Dong L, Liu Y, Chang R, Huang X, Liu Y, Wang J, Dougherty UJN: **Anti-tumour immunity controlled through mRNA m6A methylation and YTHDF1 in dendritic cells.** 2019, **566:**270-274.

20. Yang S, Wei J, Cui YH, Park G, Shah P, Deng Y, Aplin AE, Lu Z, Hwang S, He C, He YY: **m(6)A mRNA demethylase FTO regulates melanoma tumorigenicity and response to anti-PD-1 blockade.** *Nat Commun* 2019, **10:**2782.

21. Mariathasan S, Turley SJ, Nickles D, Castiglioni A, Yuen K, Wang YL, Kadel EE, Koeppen H, Astarita JL, Cubas R, et al: **TGF beta attenuates tumour response to PD-L1 blockade by contributing to exclusion of T cells.** *Nature* 2018, **554:**544-+.

22. Rosenberg JE, Hoffman-Censits J, Powles T, van der Heijden MS, Balar AV, Necchi A, Dawson N, O'Donnell PH, Balmanoukian A, Loriot Y, et al: **Atezolizumab in patients with locally advanced and metastatic urothelial carcinoma who have progressed following treatment with platinum-based chemotherapy: a single-arm, multicentre, phase 2 trial.** *Lancet* 2016, **387:**1909-1920.

23. Shi HL, Wei JB, He C: **Where, When, and How: Context-Dependent Functions of RNA Methylation Writers, Readers, and Erasers.** *Molecular Cell* 2019, **74:**640-650.

24. Yang Y, Hsu PJ, Chen YS, Yang YG: **Dynamic transcriptomic m(6)A decoration: writers, erasers, readers and functions in RNA metabolism.** *Cell Res* 2018, **28:**616-624.

25. Wilkerson MD, Hayes DN: **ConsensusClusterPlus: a class discovery tool with confidence assessments and item tracking.** *Bioinformatics* 2010, **26:**1572-1573.

26. Mo Q, Nikolos F, Chen F, Tramel Z, Lee YC, Hayashi K, Xiao J, Shen J, Chan KS: **Prognostic Power of a Tumor Differentiation Gene Signature for Bladder Urothelial Carcinomas.** *J Natl Cancer Inst* 2018, **110:**448-459.

27. Damrauer JS, Hoadley KA, Chism DD, Fan C, Tiganelli CJ, Wobker SE, Yeh JJ, Milowsky MI, Iyer G, Parker JS, Kim WY: **Intrinsic subtypes of high-grade bladder cancer reflect the hallmarks of breast cancer biology.** *Proceedings of the National Academy of Sciences of the United States of America* 2014, **111:**3110-3115.

28. Choi W, Porten S, Kim S, Willis D, Plimack ER, Hoffman-Censits J, Roth B, Cheng TW, Tran M, Lee IL, et al: **Identification of Distinct Basal and Luminal Subtypes of Muscle-Invasive Bladder Cancer with Different Sensitivities to Frontline Chemotherapy.** *Cancer Cell* 2014, **25:**152-165.

29. Marzouka NA, Eriksson P, Rovira C, Liedberg F, Sjodahl G, Hoglund M: **A validation and extended description of the Lund taxonomy for urothelial carcinoma using the TCGA cohort.** *Scientific Reports* 2018, **8**.

30. Robertson AG, Kim J, Al-Ahmadie H, Bellmunt J, Guo G, Cherniack AD, Hinoue T, Laird PW, Hoadley KA, Akbani R, et al: **Comprehensive Molecular Characterization of Muscle-Invasive Bladder Cancer.** *Cell* 2017, **171:**540-556 e525.

31. Rebouissou S, Bernard-Pierrot I, de Reynies A, Lepage ML, Krucker C, Chapeaublanc E, Herault A, Kamoun A, Caillault A, Letouze E, et al: **EGFR as a potential therapeutic target for a subset of muscle-invasive bladder cancers presenting a basal-like phenotype.** *Science Translational Medicine* 2014, **6**.

32. Kamoun A, de Reynies A, Allory Y, Sjodahl G, Robertson AG, Seiler R, Hoadley KA, Groeneveld CS, Al-Ahmadie H, Choi W, et al: **A Consensus Molecular Classification of Muscle-invasive Bladder Cancer.** *Eur Urol* 2020, **77:**420-433.

33. Jia Q, Wu W, Wang Y, Alexander PB, Sun C, Gong Z, Cheng JN, Sun H, Guan Y, Xia X, et al: **Local mutational diversity drives intratumoral immune heterogeneity in non-small cell lung cancer.** *Nat Commun* 2018, **9:**5361.

34. Newman AM, Liu CL, Green MR, Gentles AJ, Feng W, Xu Y, Hoang CD, Diehn M, Alizadeh AA: **Robust enumeration of cell subsets from tissue expression profiles.** *Nat Methods* 2015, **12:**453-457.

35. Ritchie ME, Phipson B, Wu D, Hu Y, Law CW, Shi W, Smyth GK: **limma powers differential expression analyses for RNA-sequencing and microarray studies.** *Nucleic Acids Res* 2015, **43:**e47.

36. Zhou Y, Zhou B, Pache L, Chang M, Khodabakhshi AH, Tanaseichuk O, Benner C, Chanda SK: **Metascape provides a biologist-oriented resource for the analysis of systems-level datasets.** *Nat Commun* 2019, **10:**1523.

37. Castro MA, de Santiago I, Campbell TM, Vaughn C, Hickey TE, Ross E, Tilley WD, Markowetz F, Ponder BA, Meyer KB: **Regulators of genetic risk of breast cancer identified by integrative network analysis.** *Nat Genet* 2016, **48:**12-21.

38. Yu G, Wang LG, Han Y, He QY: **clusterProfiler: an R package for comparing biological themes among gene clusters.** *OMICS* 2012, **16:**284-287.

39. Zeng Q, Liu J, Cao P, Li J, Liu X, Fan X, Liu L, Cheng Y, Xiong W, Li J, et al: **Inhibition of REDD1 Sensitizes Bladder Urothelial Carcinoma to Paclitaxel by Inhibiting Autophagy.** *Clin Cancer Res* 2018, **24:**445-459.

40. Hazra A, Gogtay N: **Biostatistics Series Module 3: Comparing Groups: Numerical Variables.** *Indian J Dermatol* 2016, **61:**251-260.

41. DeGraff DJ, Cates JM, Mauney JR, Clark PE, Matusik RJ, Adam RM: **When urothelial differentiation pathways go wrong: Implications for bladder cancer development and progression.** *Urologic Oncology-Seminars and Original Investigations* 2013, **31:**802-811.

42. Choi W, Czemiak B, Ochoa A, Su XP, Siefker-Radtke A, Dinney C, McConkey DJ: **Intrinsic basal and luminal subtypes of muscle-invasive bladder cancer.** *Nature Reviews Urology* 2014, **11:**400-410.

43. Eriksson P, Aine M, Veerla S, Liedberg F, Sjodahl G, Hoglund M: **Molecular subtypes of urothelial carcinoma are defined by specific gene regulatory systems.** *Bmc Medical Genomics* 2015, **8**.

44. Breyer J, Wirtz RM, Laible M, Schlombs K, Erben P, Kriegmair MC, Stoehr R, Eidt S, Denzinger S, Burger M, et al: **ESR1, ERBB2, and Ki67 mRNA expression predicts stage and grade of non-muscle-invasive bladder carcinoma (NMIBC).** *Virchows Archiv* 2016, **469:**547-552.

45. Dadhania V, Zhang M, Zhang L, Bondaruk J, Majewski T, Siefker-Radtke A, Guo CC, Dinney C, Cogdell DE, Zhang SZ, et al: **Meta-Analysis of the Luminal and Basal Subtypes of Bladder Cancer and the Identification of Signature Immunohistochemical Markers for Clinical Use.** *Ebiomedicine* 2016, **12:**105-117.

46. Jones RT, Felsenstein KM, Theodorescu D: **Pharmacogenomics: Biomarker-Directed Therapy for Bladder Cancer.** *Urologic Clinics of North America* 2016, **43:**77-+.

47. Lim S, Koh MJ, Jeong HJ, Cho NH, Choi YD, Cho DY, Lee HY, Rha SY: **Fibroblast Growth Factor Receptor 1 Overexpression Is Associated with Poor Survival in Patients with Resected Muscle Invasive Urothelial Carcinoma.** *Yonsei Medical Journal* 2016, **57:**831-839.

48. Liu RY, Zeng YY, Lei Z, Wang LQ, Yang HP, Liu ZY, Zhao J, Zhang HT: **JAK/STAT3 signaling is required for TGF-beta-induced epithelial-mesenchymal transition in lung cancer cells.** *International Journal of Oncology* 2014, **44:**1643-1651.

49. Gu GY, Gao TH, Zhang L, Chen XY, Pang Q, Wang YN, Wang D, Li J, Liu Q: **NKAP alters tumor immune microenvironment and promotes glioma growth via Notch1 signaling.** *Journal of Experimental & Clinical Cancer Research* 2019, **38**.

50. Karn T, Denkert C, Weber KE, Holtrich U, Hanusch C, Sinn BV, Higgs B, Jank P, Huober J, Blohmer JU, et al: **Tumour mutational burden and immune infiltration as independent predictors of response to neoadjuvant immune checkpoint inhibition in early TNBC in GeparNuevo.** *Annals of Oncology* 2020, **31:**S58-S58.

51. **TGF beta attenuates tumour response to PD-L1 blockade by contributing to exclusion of T cells %J Nature.** 2018, **554:**544-548.

52. Walshaw RC, Honeychurch J, Illidge TM, Choudhury A: **The anti-PD-1 era - an opportunity to enhance radiotherapy for patients with bladder cancer.** *Nat Rev Urol* 2018, **15:**251-259.

53. Liu X, Liu J, Xiao W, Zeng Q, Bo H, Zhu Y, Gong L, He D, Xing X, Li R, et al: **SIRT1 Regulates N(6) -Methyladenosine RNA Modification in Hepatocarcinogenesis by Inducing RANBP2-Dependent FTO SUMOylation.** *Hepatology* 2020, **72:**2029-2050.

54. Liu J, Dou X, Chen C, Chen C, Liu C, Xu MM, Zhao S, Shen B, Gao Y, Han D, He C: **N (6)-methyladenosine of chromosome-associated regulatory RNA regulates chromatin state and transcription.** *Science* 2020, **367:**580-586.

55. Zhou Z, Lv J, Yu H, Han J, Yang X, Feng D, Wu Q, Yuan B, Lu Q, Yang H: **Mechanism of RNA modification N6-methyladenosine in human cancer.** *Mol Cancer* 2020, **19:**104.

56. Huang H, Weng H, Chen J: **m(6)A Modification in Coding and Non-coding RNAs: Roles and Therapeutic Implications in Cancer.** *Cancer Cell* 2020, **37:**270-288.

57. Zhang B, Wu Q, Li B, Wang D, Wang L, Zhou YL: **m(6)A regulator-mediated methylation modification patterns and tumor microenvironment infiltration characterization in gastric cancer.** *Mol Cancer* 2020, **19:**53.

58. He L, Li H, Wu A, Peng Y, Shu G, Yin G: **Functions of N6-methyladenosine and its role in cancer.** *Mol Cancer* 2019, **18:**176.

59. Liu X, Liu J, Xiao W, Zeng Q, Bo H, Zhu Y, Gong L, He D, Xing X, Li R, et al: **SIRT1 regulates N(6) -methyladenosine RNA modification in hepatocarcinogenesis by inducing RANBP2-dependent FTO SUMOylation.** *Hepatology* 2020.

60. Mauer J, Luo X, Blanjoie A, Jiao X, Grozhik AV, Patil DP, Linder B, Pickering BF, Vasseur JJ, Chen Q, et al: **Reversible methylation of m(6)Am in the 5' cap controls mRNA stability.** *Nature* 2017, **541:**371-375.

61. Fu Y, Jia G, Pang X, Wang RN, Wang X, Li CJ, Smemo S, Dai Q, Bailey KA, Nobrega MA, et al: **FTO-mediated formation of N6-hydroxymethyladenosine and N6-formyladenosine in mammalian RNA.** *Nat Commun* 2013, **4:**1798.

62. Wei J, Liu F, Lu Z, Fei Q, Ai Y, He PC, Shi H, Cui X, Su R, Klungland A, et al: **Differential m(6)A, m(6)Am, and m(1)A Demethylation Mediated by FTO in the Cell Nucleus and Cytoplasm.** *Mol Cell* 2018, **71:**973-985 e975.

63. Zhang X, Wei LH, Wang Y, Xiao Y, Liu J, Zhang W, Yan N, Amu G, Tang X, Zhang L, Jia G: **Structural insights into FTO's catalytic mechanism for the demethylation of multiple RNA substrates.** *Proc Natl Acad Sci U S A* 2019, **116:**2919-2924.

64. Sendinc E, Valle-Garcia D, Dhall A, Chen H, Henriques T, Navarrete-Perea J, Sheng W, Gygi SP, Adelman K, Shi Y: **PCIF1 Catalyzes m6Am mRNA Methylation to Regulate Gene Expression.** *Mol Cell* 2019, **75:**620-630 e629.

65. Boulias K, Toczydlowska-Socha D, Hawley BR, Liberman N, Takashima K, Zaccara S, Guez T, Vasseur JJ, Debart F, Aravind L, et al: **Identification of the m(6)Am Methyltransferase PCIF1 Reveals the Location and Functions of m(6)Am in the Transcriptome.** *Mol Cell* 2019, **75:**631-643 e638.

66. Akichika S, Hirano S, Shichino Y, Suzuki T, Nishimasu H, Ishitani R, Sugita A, Hirose Y, Iwasaki S, Nureki O, Suzuki T: **Cap-specific terminal N (6)-methylation of RNA by an RNA polymerase II-associated methyltransferase.** *Science* 2019, **363**.

67. Sanchez-Pulido L, Andrade-Navarro MA: **The FTO (fat mass and obesity associated) gene codes for a novel member of the non-heme dioxygenase superfamily.** *BMC Biochem* 2007, **8:**23.

Figures

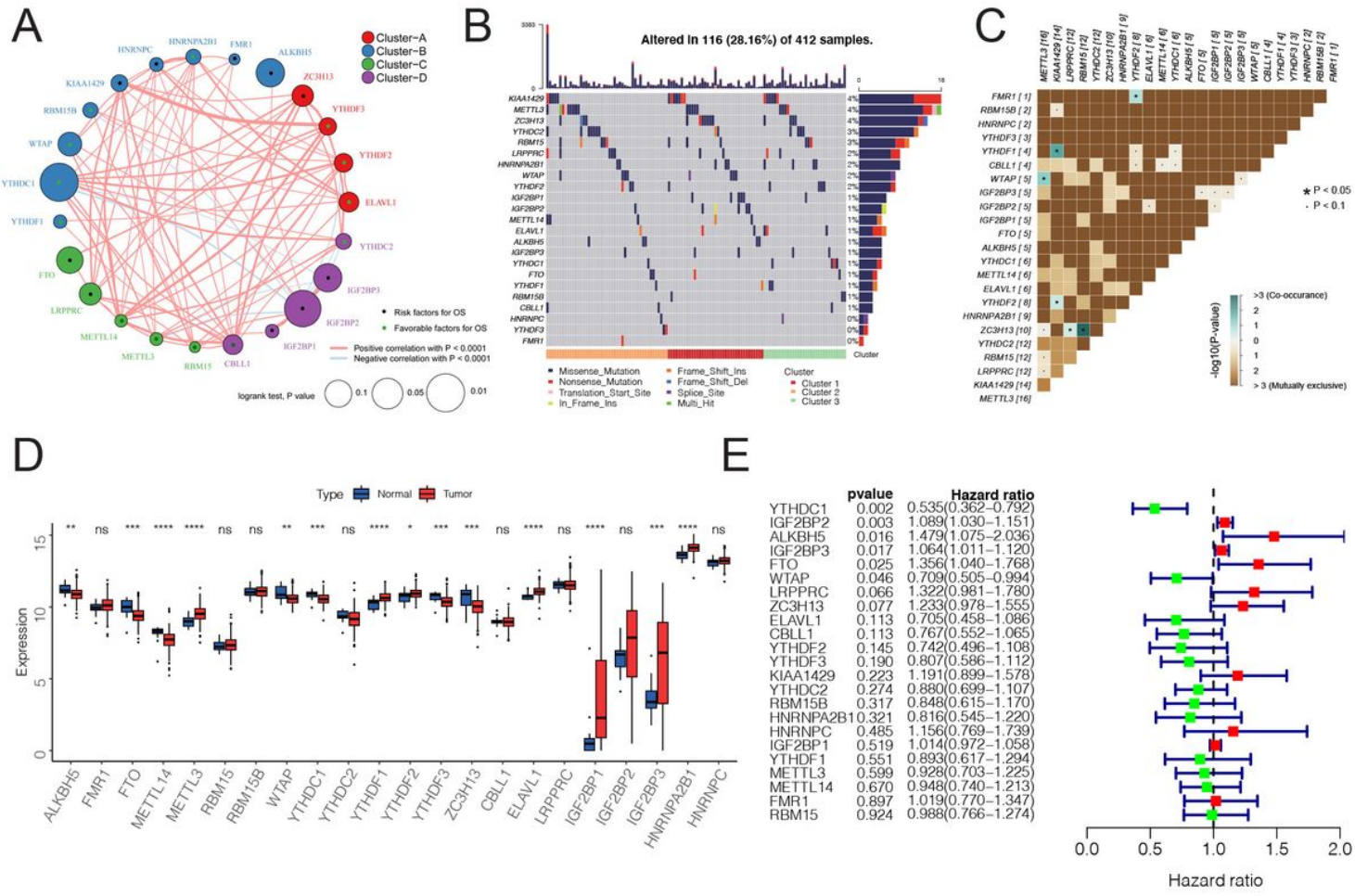

Figure 1

Genetic and expression characteristics of the 23 m6A regulatory genes in bladder cancer. A. Depending on the correlation among the 23 m6A regulatory genes, these were divided into four groups: Cluster A, red; cluster B, blue; cluster C, green; cluster D, purple. The dot in the middle of each circle represents the influence of the m6A regulator on OS, the favorable factors for OS are shown in green, and the risk

factors are shown in black. The size of each circle represents the log-rank test p-value of the influence of the m6A regulator on OS (expressed as log10 value). The line connecting the two m6A regulatory factors represents the interaction between the factors; the red connection represents the positive correlation, and the light blue represents the negative correlation between the two factors. B. Waterfall diagram showing 23 mutations of m6A regulator in bladder cancer. Each column represents the patient, and each color represents the mutation type, and gray indicates that there is no mutation in the gene in the sample. The bar graph above shows the TMB, and the number on the right shows the mutation frequency of each regulator. C. The mutation mode of 23 m6A regulatory factors; azure represents co-occurring mutations, brown represents mutually exclusive mutations, * $P < 0.05$, · $P < 0.1$. D. The expression levels of 23 m6A regulatory factors in cancer and normal tissues. Tumor, red; normal, blue. The top and bottom of the box indicate the quartile range of the value, the lines in the box represent the median value, and the black dot represents the abnormal value. *P<0.05; **P<0.01; ***P<0.001; ****P<0.0001. E. The forest map shows the univariate Cox analysis results for the impact of 23 m6A regulatory factors on the OS of bladder cancer patients. Red represents risk factors, and green represents protective factors.

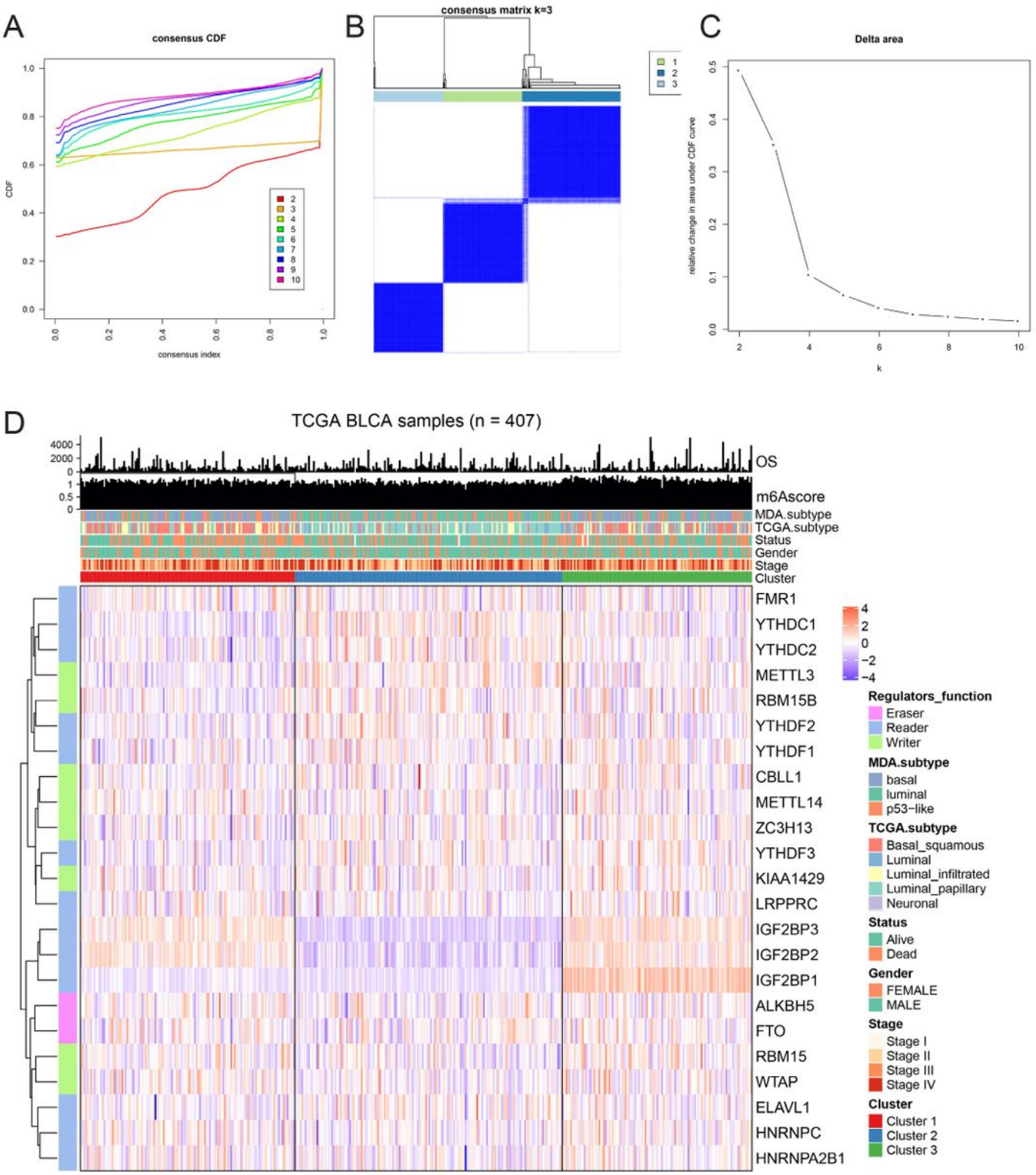

Figure 2

The expression of 23 kinds of m6A regulatory factors identified three different methylation patterns A-C. According to the expression of 23 m6A regulatory factors, we classified 407 bladder cancer patients, and 3 was the optimal cluster number.D. Heatmap display showing the expression of 23 m6A regulatory factors among three different m6A modification modes. The relationship between different m6A

modification modes and clinical features such as OS, m6Ascore, MDA typing, TCGA typing, status, gender, stage, etc.

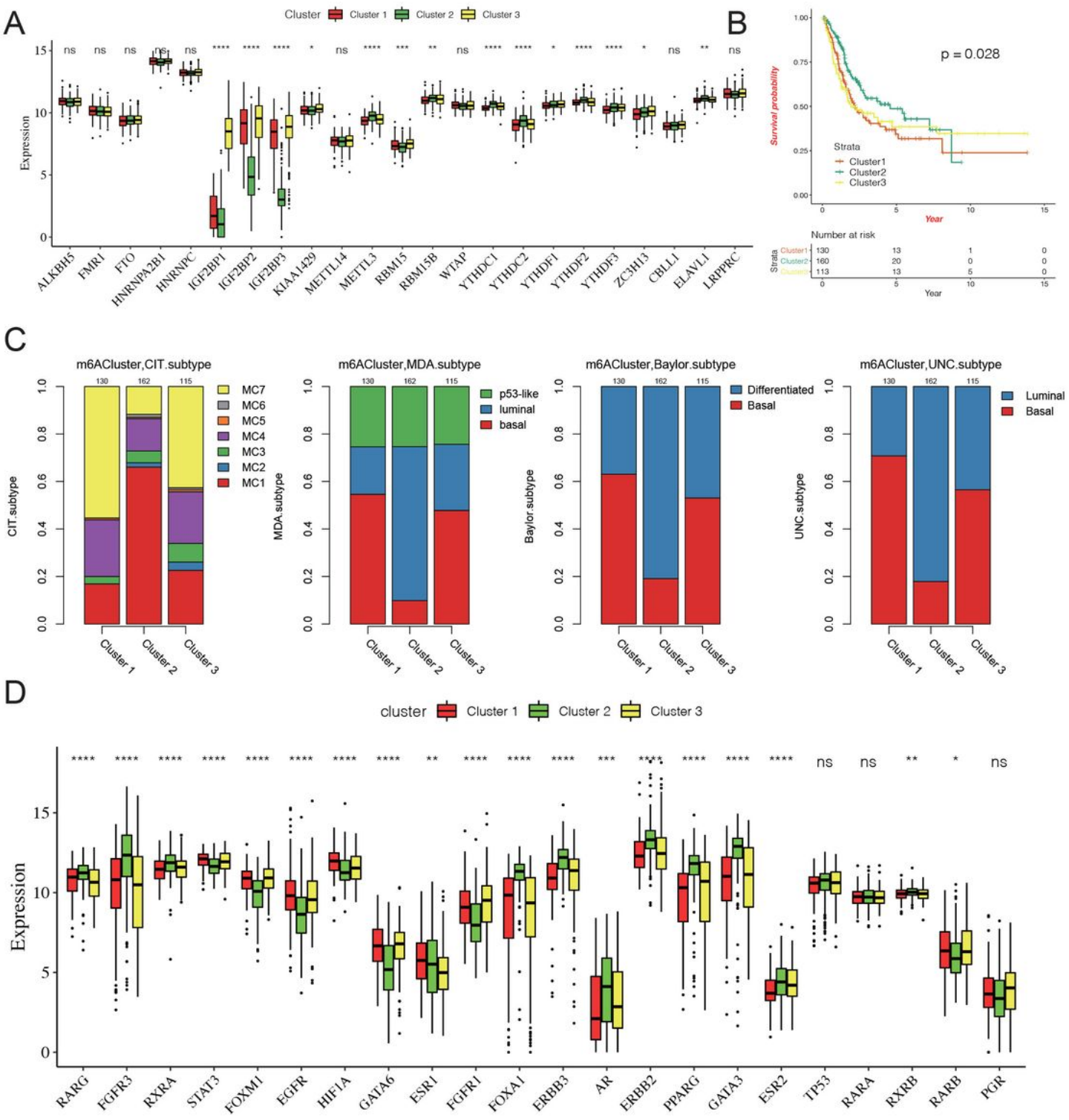

Figure 3

Characteristics of three different methylation patterns of m6A A. The expression of 23 m6A regulatory factors varied among the three different m6A modification modes. The upper and lower end of the box indicates the quartile range of the value, the lines in the box represents the median value, the black dot

represents the abnormal value, and the asterisk represents the statistical p-value, *P<0.05; **P<0.01; **P<0.001, ***P<0.0001. B.The KM curve showing the difference in the effects of the three m6A modification modes on OS. C. Comparative analysis of three different m6A modification patterns and molecular typing of bladder cancer, including Bayol classification, MDA typing, CIT Curie typing, and UNC typing. D. The upper and lower ends of the box represent the quartile range of values, the lines in the box represent the median value, and the black dots represent the abnormal values. The asterisk represents the statistical p-value, *P<0.05; **P<0.01; *P<0.001, ***P<0.0001.

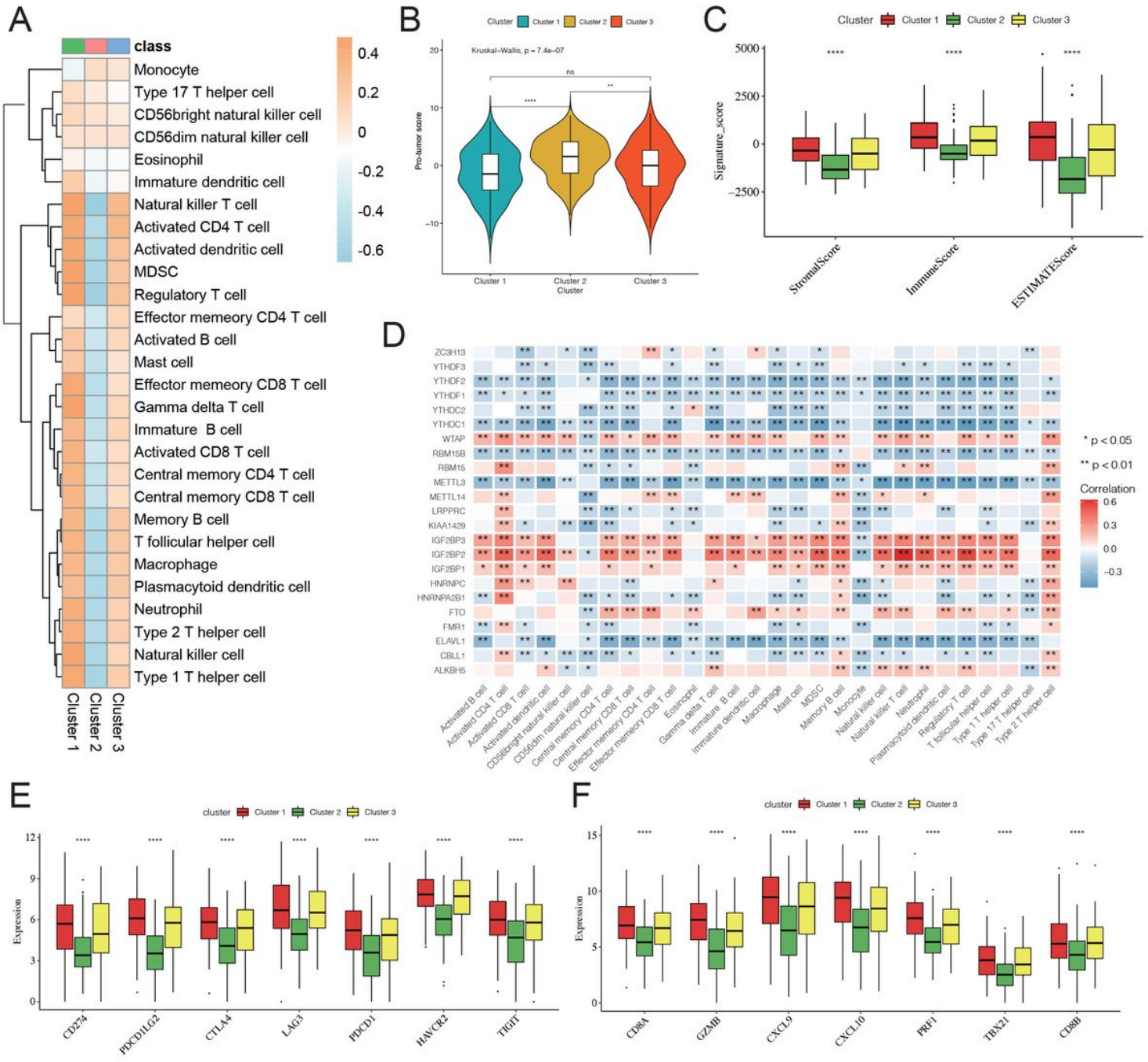

Figure 4

Effect of m6A modification on immune cell infiltration and immune checkpoint expression in the tumor immune microenvironment A. The thermogram shows the difference in the average level of 28 kinds of immune cell infiltration among three different m6A modification modes. B. The violin box chart shows the difference in Pro-tumor score, the asterisk represents the statistical p-value (*P<0.05; **P<0.01; ***P<0.001, ****P< 0.0001). C. The ESTIMATE algorithm estimates the ratio of immune and matrix components of each sample in TME. The histogram shows the difference in immune score, stromal score, and the ESTIMATE score among the three different m6A modification modes. The asterisk represents the statistical p-value(*P<0.05; **P<0.01; ***P<0.001, ****P<0.0001). D. Thermogram showing the 23 m6A regulatory factors that were correlated with 28 kinds of immune cells. The darker color indicates a higher correlation. The asterisk represents the statistical p-value (*P<0.05, **P<0.01). E-F. The Box plot shows the immune checkpoint related gene (E) and the CD8+T cell marker gene (F) among the three different m6A modification modes.

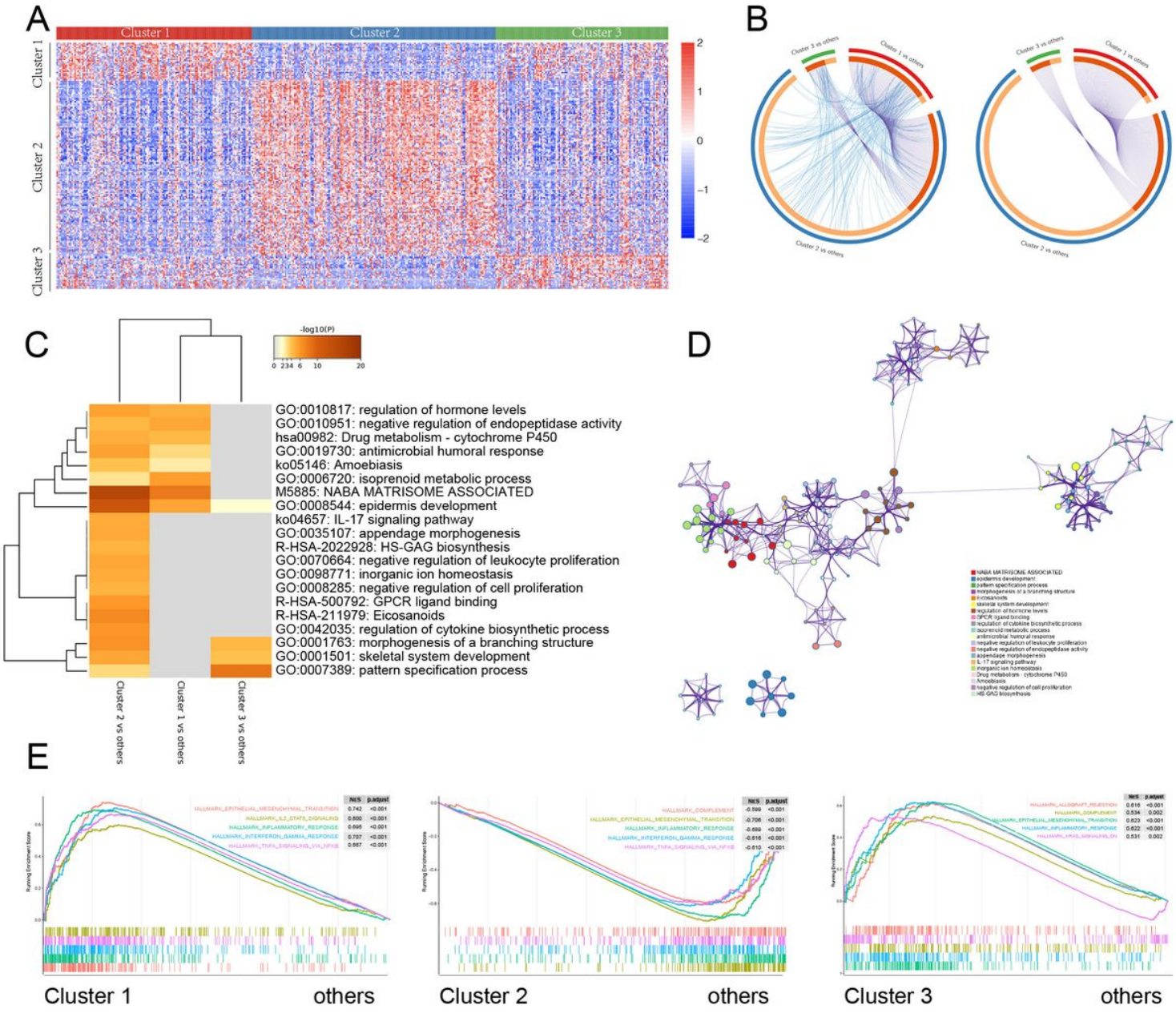

Figure 5

Enrichment of different gene signaling pathways in different m6A modification modes A. Heatmap showing the expression of different genes in three different m6A modification modes.B. Circos diagram showing the overlap of differentially expressed genes by a pairwise comparison of three different m6A modification patterns. Each arc in the outer circle represents the comparison group, and each arc in the inner circle represents a gene list. Each gene has a point on the arc. Dark orange represents the genes that appear in multiple lists, and light orange represents the only gene in the list. The purple line indicates the overlap between genes. The more purple links and the longer the dark orange arc, the higher the overlap between input gene lists, where they fall into the same ontology term (the term has to be statistically significantly enriched and with a size no larger than 100). C. The thermogram shows the enrichment of gene signaling pathways with different m6A modification modes. The heat map cells are colored by their p-values, and the white cells indicate that the term lacks enrichment in the corresponding gene list. D. Selected representative signal paths shown in a network layout. Each signal path is represented by a circular node, whose size is directly proportional to the number of input genes in the term. The color represents the cluster identity, i.e, nodes with the same color belong to the same cluster. Terms with similarity score>0.3 are linked by edges (the thickness of the edge represents the similarity score). The network was visualized using Cytoscape (v3.1.2). E. GSEA of the marker gene set downloaded from the MSigDB database. All transcripts were sequenced according to the multiple variation (log2) obtained using the different analysis among three different m6A modification modes. GSEA analysis evaluated the skewness of the two distributions of the selected gene set in the sequenced gene list.

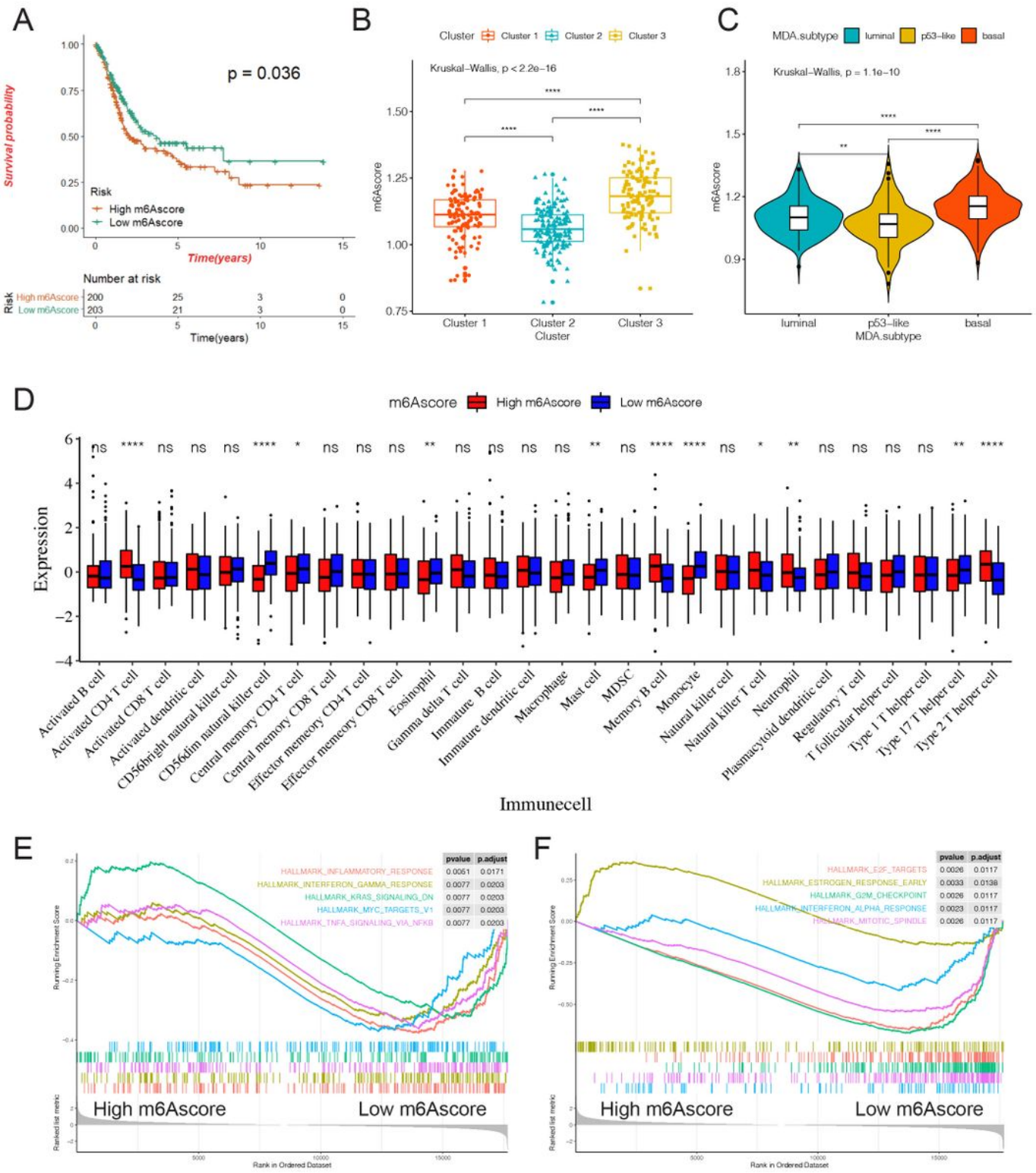

Figure 6

Relationship between m6Ascore and the characteristics of bladder cancer A.KM survival curve showing the effect of m6Ascore on OS in the TCGA-BLCA cohort. B-C.The difference of m6A score among three different m6A modification patterns (B) and MDA typing (C). The asterisk represents the statistical p-value(*P<0.05; **P<0.01; ***P<0.001, ****P< 0.0001). D. According to the expression of the m6Ascore,407 patients were classified into a high m6Ascore group and a low m6Ascore group. The histogram shows

the expression difference of 28 kinds of immune cells between the two groups. E-F. All transcripts were sequenced according to the multiple variations (log2) obtained by the two groups in the analysis. GSEA analysis evaluated the skewness of the two distributions of the selected gene set in the sequenced gene list.

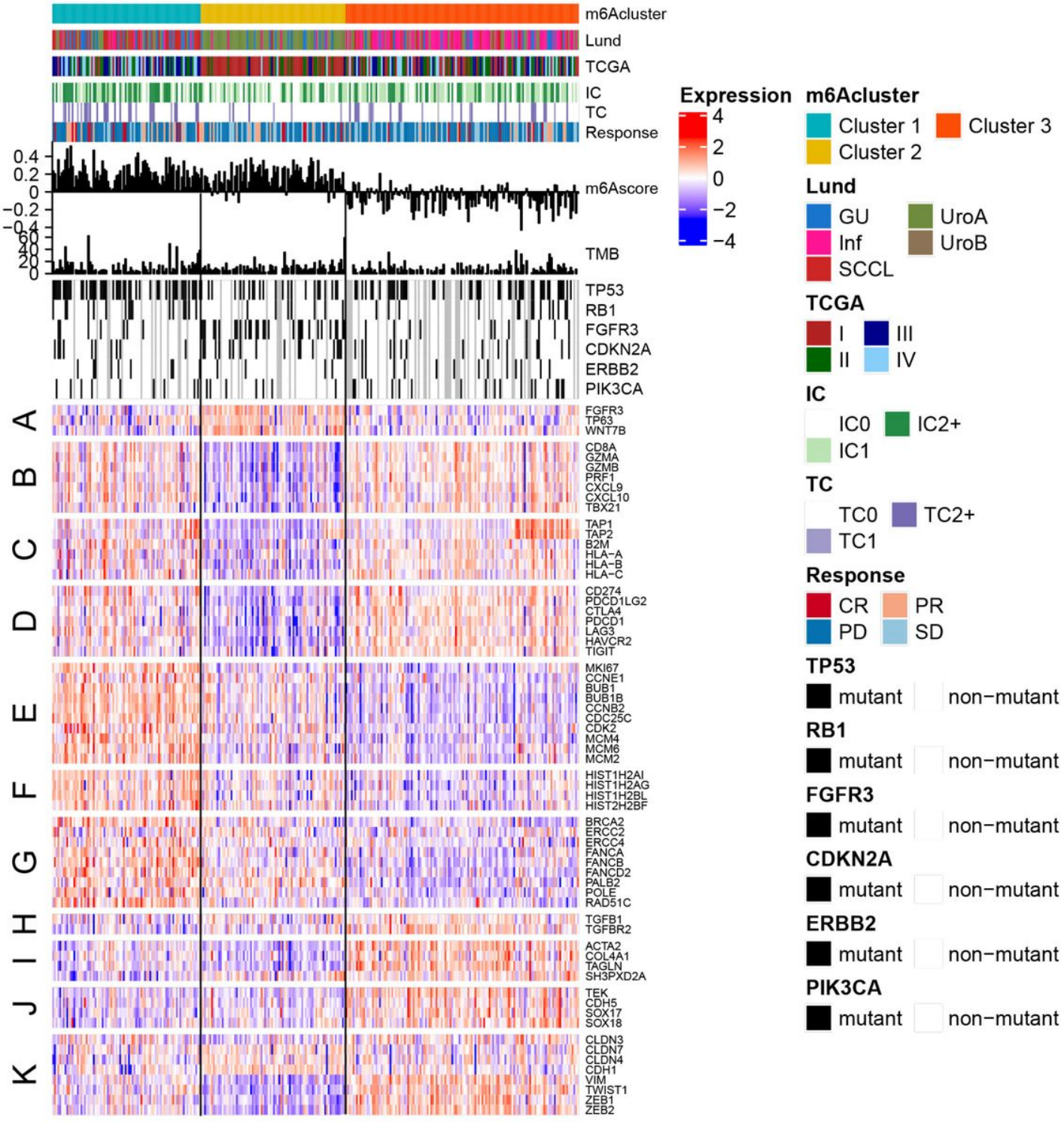

Figure 7

Characteristics of m6A modification in anti-PD-L1 immunotherapy cohort of bladder cancer Heatmap representing all patients evaluated for anti-PD-L1 response, First, the sequence was based on the

modified mode of m6A, next by the molecular subtype, PD-L1 expression on cells (IC), PD-L1 expression on cells (TC), and the reaction to atezolizumab. The m6Ascore and TMB levels of each patient are shown, and the mutation status of several genes of interest (black, mutation; gray, patients without mutation data) are shown. In addition, the lines of the heat map show the expression of the genes of interest (z-score), which are divided into the following biological classes and/or pathways: A: FGFR3 gene signature;B: CD8 Teff signature;C: antigen-processing machinery;D: immune checkpoint signature;E: MKI67 and cell cycle genes;F: DNA replication-dependent histones;G：DNA damage-repair genes;H：TGFβ receptor and ligand;I：F-TBRS genes;J：EMT markers;K：angiogenesis signature.

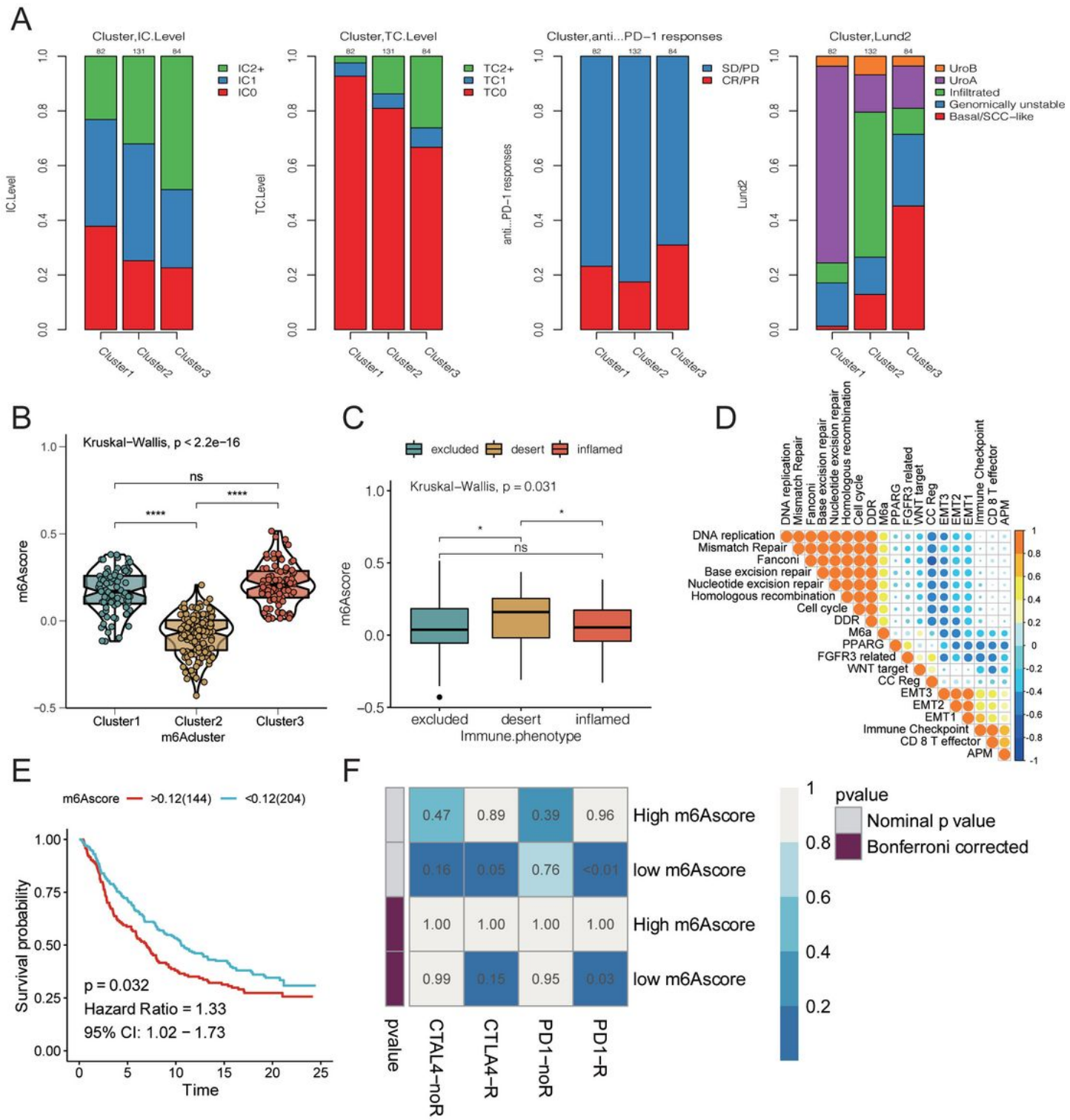

Figure 8

Effect of m6A modification mode on the treatment of bladder cancer with PD-L1 A. From left to right, the stacking histogram shows the relationship between the three kinds of m6A modification modes and PD-L1 expression on immune cells (IC), PD-L1 expression on tumor cells (TC), response to atezolizumab, and Lund typing. B. m6Ascore difference between 3 different m6A modification modes. The asterisk represents the statistical p-value (*P<0.05; **P<0.01; ***P<0.001, ****P<0.0001). C. The difference in

m6Ascore among the three immunophenotypes; the asterisk represents the statistical p-value (*P<0.05; **P<0.01; ***P<0.001, ****P<0.0001). D. Spearman correlation was used to analyze the relationship between the m6Ascore and known gene characteristics in the IMvigor 210 cohort. The larger the circle, the higher the correlation. E. KM curve showing the effect of m6Ascore on OS in the IMvigor210 cohort. F. Using the SubMAP algorithm, we inferred the possibility of anti-PD1 and anti- cytotoxic T-lymphocyte-associated protein 4 (CTLA4) response immunotherapy in the high and low m6Ascore groups. High ICscore group may respond better to PD-1 treatment (Bonferroni-corrected P = 0.03)

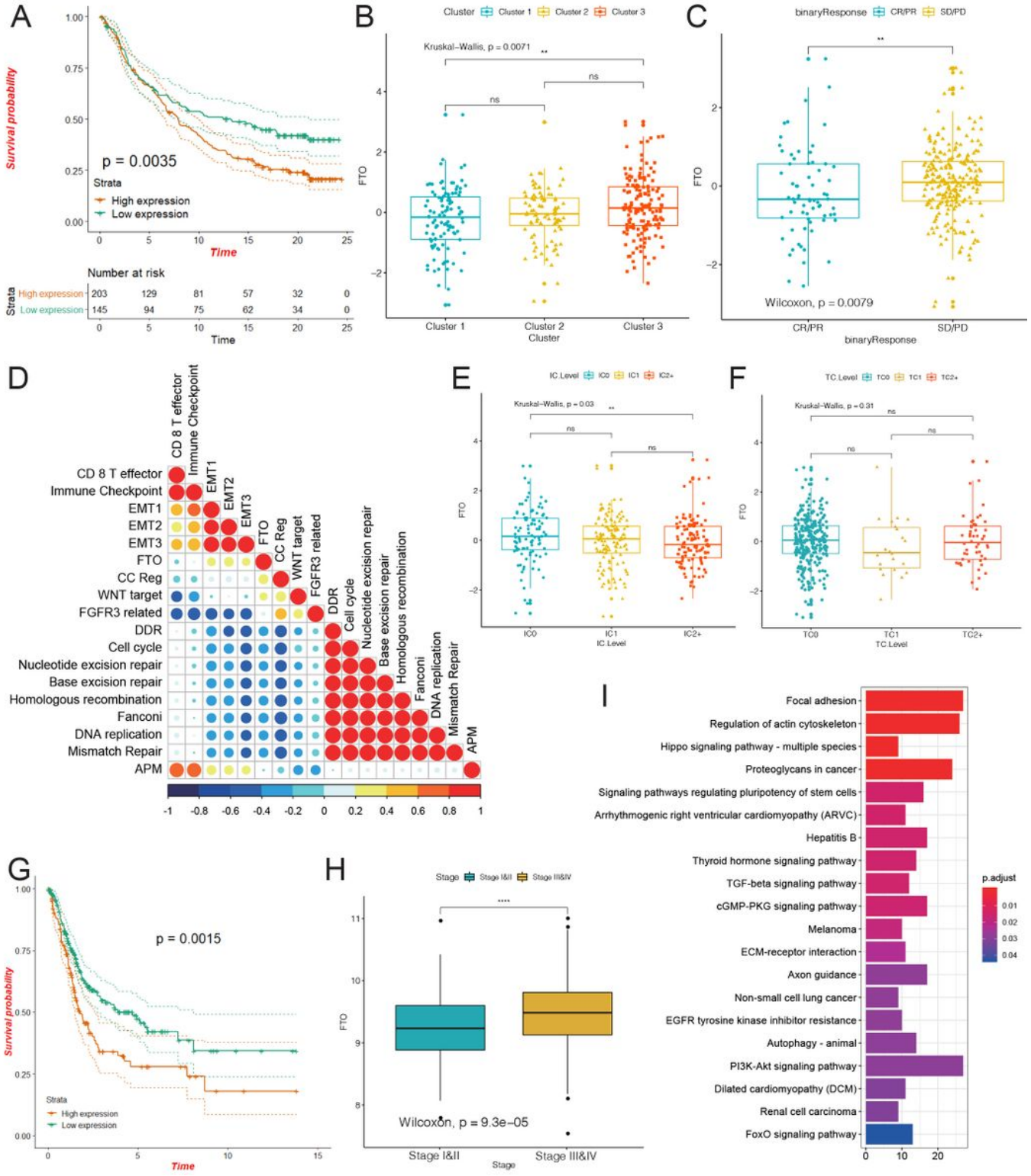

Figure 9

Characteristics of FTO in the TCGA-BLCA cohort and anti-PD-L1 treatment cohort A. KM curve showing the effect of FTO on OS in the IMvigor 210 cohort. B The difference in FTO expression among the three different m6A modification patterns in the IMvigor 210 cohort; the asterisk represents the statistical p-value (*P<0.05; **P<0.01; ***P<0.001, ****P<0.0001). C The difference in FTO expression between responders (CR/PR) and non-responders (SD/PD) in the IMvigor 210 cohort; the asterisk represents the statistical p-value (*P<0.05; **P<0.01; ***P<0.001, ****P<0.0001). D Spearman's correlation was used to analyze the correlation between FTO expression and known gene characteristics in the IMvigor 210 cohort. Blue, negatively correlated; orange, positively correlated; and the larger circle indicates a higher correlation. E-F. The relationship between FTO expression and PD-L1 expression on in immune cells(IC), and PD-L1 expression in tumor cells (TC). The asterisk represents the statistical p-value (*P<0.05; **P<0.01; ***P<0.001, ****P<0.0001). G KM curve showing the effect of FTO on OS in the TCGA-BLCA cohort. H Box plot showing the difference in FTO expression between stage I and II and stage III and IV; the asterisk represents the statistical p-value (*P<0.05; **P<0.01; ***P<0.001, ****P<0.0001). I Pearson correlation was used to calculate the correlation between FTO and all other protein-coding genes, and genes with a correlation coefficient R>=0.03, and p<0.05 were selected as FTO-related genes. These genes were enriched by KEGG signaling pathway analysis to study FTO function.

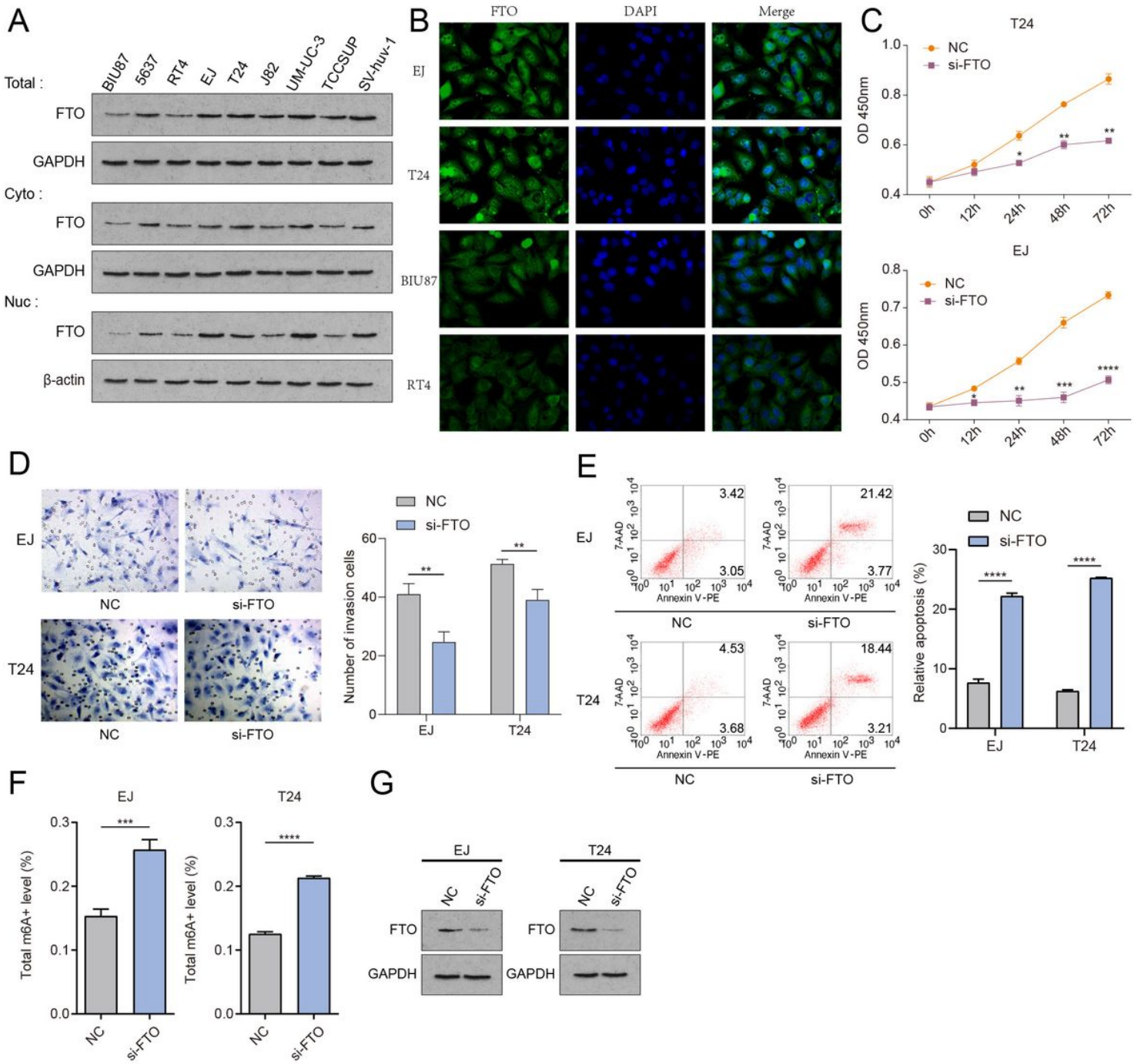

Figure 10

FTO may be involved in the occurrence and development of bladder cancer in vitro A. WB method to detect nuclear, cytoplasmic and overall expression levels in BIU87 cells, 5637 cells, T24 cells, EJ cells, RT4 cells, J82 cells, UM-UC-3 cells, TCCSUP cells, and human bladder epithelial immortalized SV-huv-1 cells B. IF immunofluorescence method to detect the cellular localization of FTO protein. C. CCK-8 to detect the proliferation level of each group of cells D. Transwell method to observe the invasion level of each group of cells E. Flow cytometry method to detect apoptosis in each group F. Detection of m6A enzyme activity level in each group G. WB method to detect the FTO expression level after siRNA knockdown

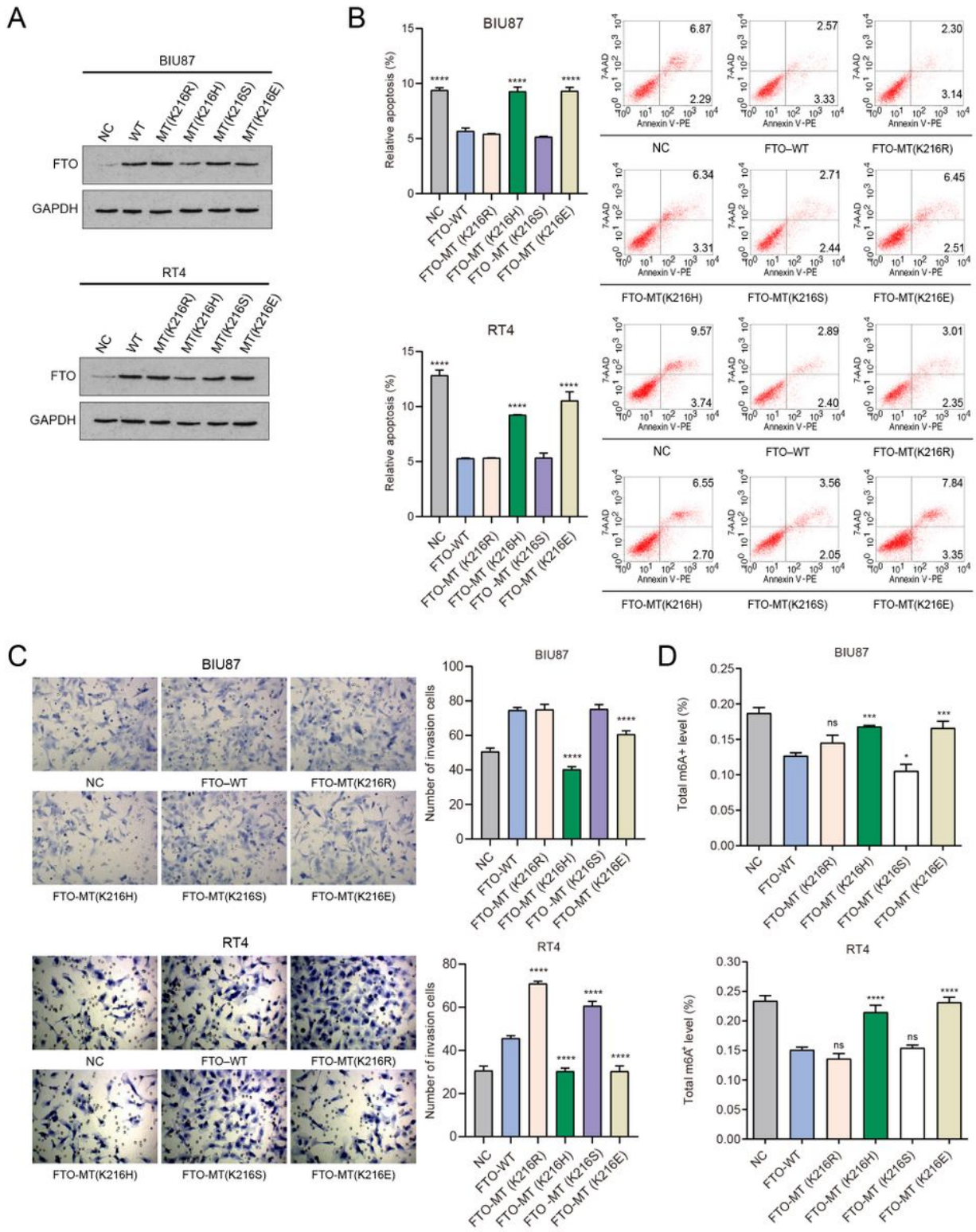

Figure 11

K216H and K216E may be important targets for regulating FTO A. WB method to detect the expression level of FTO in each group B. Flow cytometry method to detect apoptosis in each group of cells C. Transwell method to observe the level of cell invasion in each group D. Detection of m6A enzyme activity in each group

Supplementary Files

This is a list of supplementary files associated with this preprint. Click to download.

- SupplementaryFig.1.pdf
- SupplementaryFig.2.pdf
- SupplementaryFig.3.pdf
- SupplementaryFig.4.pdf
- SupplementaryFig.5.pdf
- SupplementaryFig.6.pdf
- SupplementaryFig.7.pdf
- Supplementarytable.xlsx